

# Field measurements and hydrodynamic modelling to evaluate the importance of factors controlling overwash

Ana Matias<sup>1</sup>, Ana Rita Carrasco<sup>1</sup>, Carlos Loureiro<sup>1,2,3</sup>, Gerd Masselink<sup>4</sup>, Umberto Andriolo<sup>5</sup>, Robert McCall<sup>6</sup>, Óscar Ferreira<sup>1</sup>, Theocharis A. Plomaritis<sup>1,7</sup>, André Pacheco<sup>1</sup>, Martha Guerreiro<sup>8</sup>

<sup>1</sup>CIMA -Universidade do Algarve, Campus de Gambelas, 8000 Faro, Portugal;

<sup>2</sup>Biological and Environmental Sciences, University of Stirling, Stirling, FK9 4LA, U.K.;

<sup>3</sup>School of Agricultural, Earth and Environmental Sciences, University of KwaZulu-Natal, Durban, 4001, South Africa;

<sup>4</sup>School of Biological and Marine Sciences, University of Plymouth, PL4 8AA, U.K.;

<sup>5</sup>INESC -Institute for Systems Engineering and Computers, University of Coimbra, Coimbra, Portugal;

<sup>6</sup>Deltares, Boussinesqweg 1, Delft 2629 HD, The Netherlands;

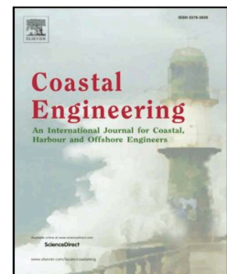
<sup>7</sup> Faculty of Marine and Environmental Science, Department of Applied Physics, University of Cadiz, Campus Rio San Pedro (CASEM), Puerto Real 11510, Cadiz, Spain;

<sup>8</sup>Instituto Hidrográfico, R. das Trinas, 49, 1249-093 Lisboa, Portugal.

## Coastal Engineering

Volume 152, Art. no. 103523, 19 p.

DOI: [10.1016/j.coastaleng.2019.103523](https://doi.org/10.1016/j.coastaleng.2019.103523)



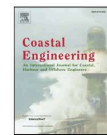
Coastal Engineering 152 (2019) 103523



Contents lists available at [ScienceDirect](https://www.sciencedirect.com)

Coastal Engineering

journal homepage: [www.elsevier.com/locate/coastaleng](http://www.elsevier.com/locate/coastaleng)



Field measurements and hydrodynamic modelling to evaluate the importance of factors controlling overwash



Ana Matias<sup>a,\*</sup>, Ana Rita Carrasco<sup>a</sup>, Carlos Loureiro<sup>a,b,c</sup>, Gerd Masselink<sup>d</sup>, Umberto Andriolo<sup>e</sup>, Robert McCall<sup>f</sup>, Óscar Ferreira<sup>a</sup>, Theocharis A. Plomaritis<sup>a,g</sup>, André Pacheco<sup>a</sup>, Martha Guerreiro<sup>h</sup>

<sup>a</sup> CIMA -Universidade do Algarve, Campus de Gambelas, 8000, Faro, Portugal

<sup>b</sup> Biological and Environmental Sciences, University of Stirling, Stirling, FK9 4LA, UK

<sup>c</sup> School of Agricultural, Earth and Environmental Sciences, University of KwaZulu-Natal, Durban, 4001, South Africa

<sup>d</sup> School of Biological and Marine Sciences, University of Plymouth, PL4 8AA, UK

<sup>e</sup> INESC - Institute for Systems Engineering and Computers, University of Coimbra, Coimbra, Portugal

<sup>f</sup> Deltares, Boussinesqweg 1, Delft, 2629, HD, the Netherlands

<sup>g</sup> Faculty of Marine and Environmental Science, Department of Applied Physics, University of Cadiz, Campus Rio San Pedro (CASEM), Puerto Real, 11510, Cadiz, Spain

<sup>h</sup> Instituto Hidrográfico, R. das Trinas, 49, 1249-093, Lisboa, Portugal

This post-print author's version of the manuscript is licensed under a [Creative Commons Attribution-NonCommercial-NoDerivatives 4.0 International License](https://creativecommons.org/licenses/by-nc-nd/4.0/).



## Highlights

- Fieldwork was undertaken during overwash to measure hydrodynamic variables
- Video data was used to measure runup and overwash
- The XBeach model in non-hydrostatic mode was setup with good predictive skills
- Modelling results were used to evaluate the relative importance on overwash prediction of the natural local variability of wave height and period, lagoon water level, nearshore bathymetry and grain-size



31 barrier island. Fieldwork was undertaken on Barreta Island (Portugal) in  
32 December 2013, during neap tides and under energetic conditions, with significant  
33 wave height reaching 2.6 m. During approximately 4 hours, more than 120 shallow  
34 overwash events were measured with a video - camera, a pressure transducer and  
35 a current-meter. This high-frequency fieldwork dataset includes runup, overwash  
36 number, depth and velocity. Fieldwork data along with information from literature  
37 were used to implement XBeach model in non-hydrostatic mode (wave-resolving).  
38 The baseline model was tested for six verification cases; the model was able to  
39 predict overwash in five. Based in performance metrics and the verification cases,  
40 it was considered that the Barreta baseline overwash model is a reliable tool for  
41 the prediction of overwash hydrodynamics. The baseline model was then forced to  
42 simulate overwash under different hydrodynamic conditions (waves and lagoon  
43 water level) and morpho-sedimentary settings (nearshore topography and beach  
44 grain-size), within the range of values characteristic for the study area. Based on  
45 this study, the order of importance of factors controlling overwash predictability in  
46 the study area are: 1<sup>st</sup>) wave height (more than wave period) can promote  
47 overwash 3-4 times more intense than the one recorded during fieldwork; 2<sup>nd</sup>)  
48 nearshore bathymetry, particularly shallower submerge bars, can promote an  
49 average decrease of about 30% in overwash; 3<sup>rd</sup>) grain-size, finer sediment  
50 produced an 11% increase in overwash due to reduced infiltration; and 4<sup>th</sup>) lagoon  
51 water level, only negligible differences were evidenced by changes in the lagoon  
52 level. This implies that for model predictions to be reliable, accurate wave forecast  
53 are necessary and topo-bathymetric configuration needs to be monitored  
54 frequently.

55

56 Key-words: storm impacts; hydrodynamics; XBeach; runup; nearshore  
57 topography; video data.

58

## 59 1. INTRODUCTION

60 Overwash is the discontinuous transport of seawater and sediment over the barrier  
61 crest generated by wave runup (Matias and Masselink, 2017). Overwash episodes  
62 during storms are commonly described in the literature, with occurrences  
63 associated to offshore significant wave heights ranging from around 4 m  
64 (Leatherman, 1976) to more than 9 m (FitzGerald et al., 1994). However, overwash  
65 can also occur during non-storm conditions (Matias et al., 2009). Overwash  
66 associated with major storms can be catastrophic, but repeated overwash processes  
67 are fundamental for long-term natural evolution of transgressive barrier islands,  
68 whereby the net volume of sand contained in the barrier structure is often  
69 maintained whilst the barrier environments migrate landward (e.g. Dolan and  
70 Godfrey, 1973).

71 Field observations are occasionally carried out during overwash episodes, but most  
72 often, such observations are made before and after overwash occurrence (e.g. Cleary  
73 et al., 2001; Stone et al., 2004; Stockdon et al., 2009). Overwash field investigations  
74 primarily measure morphological changes induced by overwash; yet, only a limited  
75 number of studies have also measured overwash hydrodynamics. Moreover,  
76 hydrodynamic datasets are mixed in quality and scope, ranging from single  
77 hydrodynamic measurements using relatively crude methods (e.g. timing floating  
78 objects; Bray and Carter, 1992) to more comprehensive and sophisticated  
79 approaches (e.g. laser scanners; Almeida et al., 2017). To overcome logistical and  
80 technical field limitations, research efforts have been devoted to the investigation of  
81 overwash in laboratory experiments, mainly small-scale experiments (e.g. Figlus et  
82 al., 2011; Baldock et al., 2005), but also large-scale experiments (Matias et al., 2012,  
83 2013).

84 Because field measurements are scarce and difficult to obtain, and laboratory  
85 datasets may have scale and applicability limitations, reliable numerical models  
86 simulating overwash are valuable to complement field data (e.g. Martins et al.,  
87 2017), particularly in extreme wave conditions. More importantly, models can be  
88 used as predictive tools, which are crucial to manage coastal areas where overwash  
89 is not desirable, to reduce its negative consequences, to assess coastal hotspots and  
90 to evaluate and improve coastal defence designs. Recent studies report similar  
91 prediction capabilities of runup by using process oriented numerical models and  
92 empirical formulations (Vousdouskas et al. 2012; Stockdon et al. 2014; Lerma et al.,  
93 2017, Atkinson et al. 2017). Conceptually, if the dominant physical relations are well  
94 described, process-based models can provide an improvement over empirical  
95 models in conditions that are dissimilar to those used to derive those empirical  
96 models, thereby extending the range of conditions and areas of application where  
97 predictions can be made. In recent years, advancements have been made in the  
98 development and improvement of process-based models for storm impact and  
99 overwash on sandy coasts, particularly the XBeach numerical model, developed by  
100 Roelvink et al. (2009, 2017). Most overwash validation work has been limited to  
101 comparisons of morphological changes (e.g., Lindemer et al., 2010; McCall et al.,  
102 2010; De Vet et al., 2015; Muller et al., 2017), and only a few studies have  
103 demonstrated XBeach's ability to reproduce hydrodynamic processes (McCall et al.,  
104 2014 and Almeida et al., 2017 on gravel barriers and Baumann et al. 2017 on a sandy  
105 barrier). Many experimental results have already been collected, but field data of  
106 storm events, with well-documented pre-existing conditions, hydrodynamic  
107 boundary conditions of waves, wind and surge, and the storm morphological impact

108 measured directly after the storm, are still needed to validate models on the  
109 prototype scale (van Dongeren et al., 2017).

110 In this work, the results of fieldwork measurements during an overwash episode are  
111 described in detail, including the hydrodynamic variables, namely waves, tides,  
112 overwash flow properties and runup, as well as morphosedimentary measurements  
113 such as topography, bathymetry, and grain-size. Using data from the field site,  
114 XBeach model was implemented to simulate the observed overwash occurrence,  
115 and the model performance for overwash hydrodynamics was evaluated and  
116 validated with additional fieldwork measurements. The primary objective of this  
117 work is to develop a reliable model for overwash prediction in the study area and to  
118 explore the model to evaluate the role of several factors that locally influence  
119 overwash hydrodynamics (waves and water levels, nearshore morphology and  
120 grain-sizes) on a low-lying barrier island.

121

122

## 123 **2. STUDY AREA**

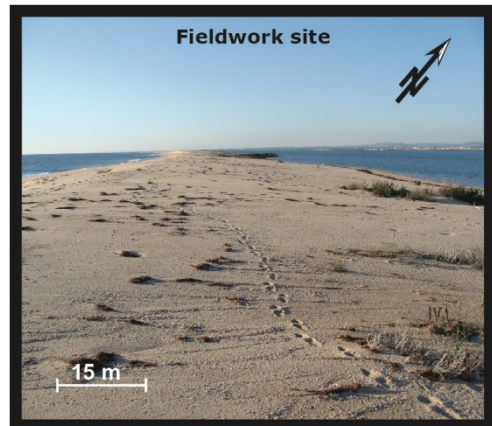
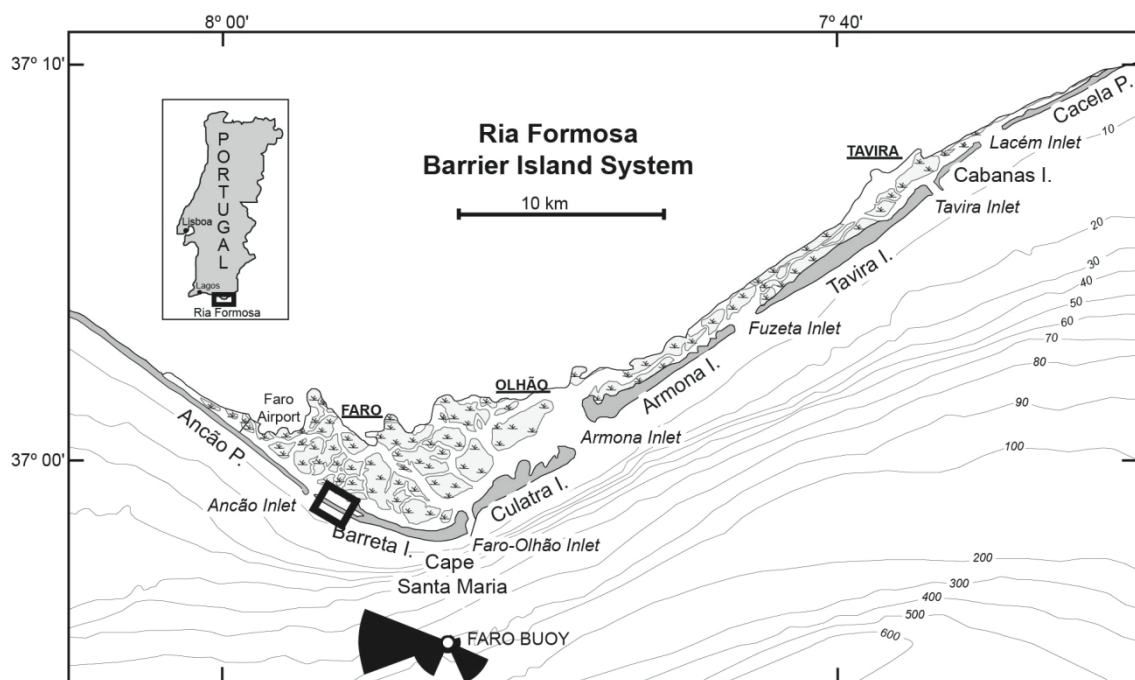
124 Fieldwork was performed on the western part of Barreta Island, located in the Ria  
125 Formosa, southern Portugal (Figure 1), a multi-inlet island system that extends for  
126 55 km along the coast. In December 2013, the field site was located about 1300 m  
127 downdrift from Ancão Inlet (Figure 1), which has a northwest to southeast  
128 migration trend with very fast rates (40-200 m/year; Vila-Concejo et al., 2002) and  
129 was migrating towards the fieldwork site between 1997 and 2015. The fieldwork  
130 site is only about 300 m from the easternmost known position of Ancão Inlet since  
131 1947 (Vila-Concejo et al., 2006). The evolution of Ancão Inlet and Barreta Island are

132 strongly interconnected, with low-volume island states associated with sediment  
133 starvation due to the updrift trap effect of the inlet (Matias et al., 2009), while high-  
134 volume states at Barreta Island relate to the incorporation of swash bars from the  
135 inlet ebb-delta (Vila-Concejo et al., 2006). At the fieldwork site, dune vegetation  
136 development on small incipient dunes was noted since 2001, with remnants still  
137 visible close to the backbarrier (Figures 1 and 2).

138

139

140



141

142 **Figure 1 – Top: Fieldwork location within the Ria Formosa barrier island system, Algarve, Portugal.**  
143 **Bottom left: Aerial photograph from 2013 showing the study area location on the Western part of**  
144 **Barreta Island, and Ancão Inlet. Bottom right: Ground picture of the study area looking Westwards,**  
145 **with the lagoon and mainland to the right-hand side.**

146

147 The Ria Formosa barrier system is in a mesotidal regime, with a mean tidal range of  
148 about 2 m that can reach up to 3.5 m during spring tides. The return period of a  
149 storm surge with a water level of 2.23 m above Mean Sea Level (MSL) in Lagos (70  
150 km west of the study area) is 10 years (Gama et al., 1994). The offshore wave climate  
151 in this area is dominated by W-SW waves (71% of occurrences), while short-period  
152 SE waves generated by regional winds occur during 23% of the time (Costa et al.,  
153 2001). Wave energy is moderate with an average annual significant wave height  
154 ( $H_s$ ) of 1.0 m and average peak period ( $T_p$ ) of 8.2 s (Costa et al., 2001). Storm events  
155 in the region were define as events with  $H_s$  above 3 m (Pessanha and Pires, 1981).  
156 According to Costa et al. (2001), a storm from West with  $H_s$  of 3–5 m has an annual  
157 probability of 0.2% for  $T_p = 7-11$  s, and of 0.1% for  $T_p = 11-15$  s. The western section  
158 of Barreta Island has a NW-SE orientation, such that it is directly exposed to W-SW  
159 waves, and it is relatively protected from SE waves (Figure 1).

160

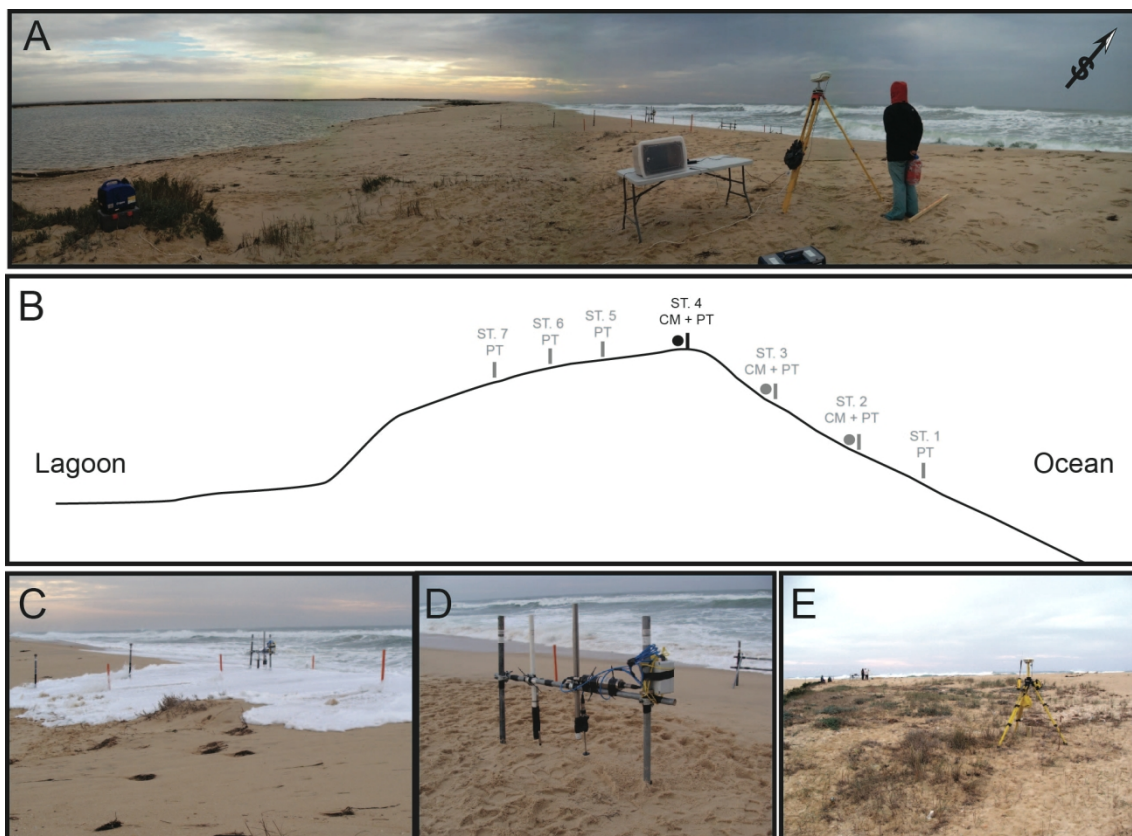
161

### 162 **3. FIELDWORK MEASUREMENTS**

163 A fieldwork campaign was conducted at the study site during a period expected to  
164 lead to overtopping based on storm wave forecasts and previous knowledge of  
165 barrier morphology. During this campaign, which took place on the 12<sup>th</sup> of  
166 December 2013, data was collected between 08:00 and 13:00, when an overwash

167 episode was observed. Measurements were undertaken along a single cross-shore  
168 profile in a low-lying section of the barrier, where overwash was expected to occur  
169 (Figures 1 and 2A). The selected profile is located on bare sand, but westwards there  
170 are remnants of former dunes (Figure 2E), where a control station and campsite  
171 were placed and the GPS base unit established.

172



173

174 **Figure 2 – Fieldwork settings. A: Overview of barrier measuring stations and video monitoring**  
175 **system. B: Location of measuring stations across the barrier island. C: Overwash over the barrier**  
176 **crest, with water reaching stations ST4, ST5, and ST6. D: Detail of measuring station ST4, with the**  
177 **electromagnetic current-meter and data-logger (right hand-side) and the pressure transducers (left-**  
178 **hand side). E: View over the remnants of dune vegetation located westward of the measuring profile,**  
179 **and the base unit of the DGPS.**

180

181

### 182 3.1. OFFSHORE AND NEARSHORE WAVES AND TIDES

183 Offshore waves during the fieldwork campaign were recorded by a directional wave  
184 buoy (Datawell Waverider), operated by the Hydrographic Institute of the  
185 Portuguese Navy, and located approximately 8 km from the fieldwork site in 93 m  
186 water depth (Figure 1). The wave spectrum was computed internally for sequential  
187 periods of 30 minutes and transmitted to a land station, where it was quality  
188 checked. To obtain the wave conditions in the nearshore area of the study site, the  
189 numerical wave propagation model SWAN (Simulating WAVes Nearshore; Booij et  
190 al., 1999; Ris et al., 1999) was used. SWAN was run in third generation, 2D stationary  
191 mode, and implemented using a nested modelling scheme, with two model domains  
192 composed by a 20-m resolution local grid, nested into the 50-m resolution regional  
193 grid. Simulations were forced at the offshore boundary of the regional grid with the  
194 measured 2D spectra from the wave buoy, variable water levels and wind forcing  
195 obtained from the nearby Faro Airport (location in Figure 1). SWAN's default  
196 parameters for wave growth, whitecapping dissipation, depth-induced breaking  
197 according to the  $\beta$ -kd model for surf-breaking (Salmon and Holhuijsen, 2015), triad  
198 and quadruplet wave-wave interactions, were used for all simulations. Bottom  
199 friction dissipation was included using the model of Smith et al. (2011), which  
200 considers bottom friction as dependent on the formation of seabed ripples and  
201 sediment size (set according to measurements in the area; section 3.3).

202 Tidal levels in the ocean margin were calculated with an algorithm developed by  
203 Pacheco et al. (2014); which computes the astronomical constituents with a tidal-  
204 analysis toolbox (Pawlowicz et al., 2002) over an hourly time-series for the period  
205 2003–2010 from a tide gauge located on Faro-Olhão Inlet (about 6 km eastwards of  
206 the study area; Figure 1). Tidal levels on the lagoon margin were determined using  
207 an estimate of the time delay and level shift between oceanic and lagoon tidal levels

208 for this area. The delay and shift were calculated from water level data collected by  
209 Popesso et al. (2016). Storm surge values, which were small during this event  
210 compared to the astronomic tide, were obtained from the closest operational tidal  
211 gauge located in Huelva, Spain (60 km to the East; Puertos de Estado; url:  
212 <http://www.puertos.es/es-es/oceanografia>).

213

### 214 **3.2. OVERWASH HYDRODYNAMICS AND RUNUP**

215 The field monitoring system was composed of seven measuring stations (ST) with  
216 sets of instruments (current-meters CM and pressure transducers PT) deployed  
217 along a cross-shore profile (Figure 2B). Stations were numbered from the low-tide  
218 water level at the beach (ST 1 in Figure 2) to the barrier crest (ST 4; Figures 2C and  
219 2D) ending at the backbarrier section, above the lagoon high-water level (ST 7). PTs  
220 measuring at 4 Hz were placed at all STs and CMs were placed at ST 2, ST 3 and ST  
221 4. Due to intense erosion during high-tide, ST1 and ST 2 collapsed and ST 3 was  
222 damaged. The only operational current meter for the entire duration of the  
223 campaign was an electromagnetic current meter (Midas from Valeport, with  
224 measuring range  $0 - 5 \text{ ms}^{-1}$ ) at ST 4 (located on the barrier crest). This means that  
225 it was impossible to record in-situ swash depth and velocity at the beach face.

226 During the measured overwash episode a number of overwash events, defined as a  
227 single passage of water above the barrier crest, were recorded. Since all instruments  
228 were synchronized and calibrated for atmospheric pressure in the field, overwash  
229 events were identified and isolated using time tagging. Overwash depths for each  
230 event were determined using pressure data from the PT measuring stations and  
231 overwash event velocity at crest computed from the electromagnetic CM data.

232 Maximum overwash depth and peak velocity at the barrier crest were calculated for  
233 each overwash event. Decreasing overwash depth landward of the barrier crest  
234 (from PTs at stations ST5, ST6, and ST7) were discarded, as measurements failed  
235 the quality checks. This is likely due to technical limitations in measuring  
236 intermittent, short duration, very shallow flows (estimation of less than 5 mm),  
237 which characterize overwash events at these locations.

238 The overwash episode was also monitored by a video camera, acquiring imagery at  
239 10 Hz, mounted on a tripod looking sideways at the instrumented cross-shore  
240 profile (Figure 2A). The elevation of the camera sensor was 4.9 m above MSL. All  
241 instruments and Ground-Control Points (GCP; red poles in Figure 2C as examples)  
242 for video analysis were geo-referenced with an RTK-DGPS (Real Time Kinematics  
243 Differential Global Positioning System; Figure 2E).

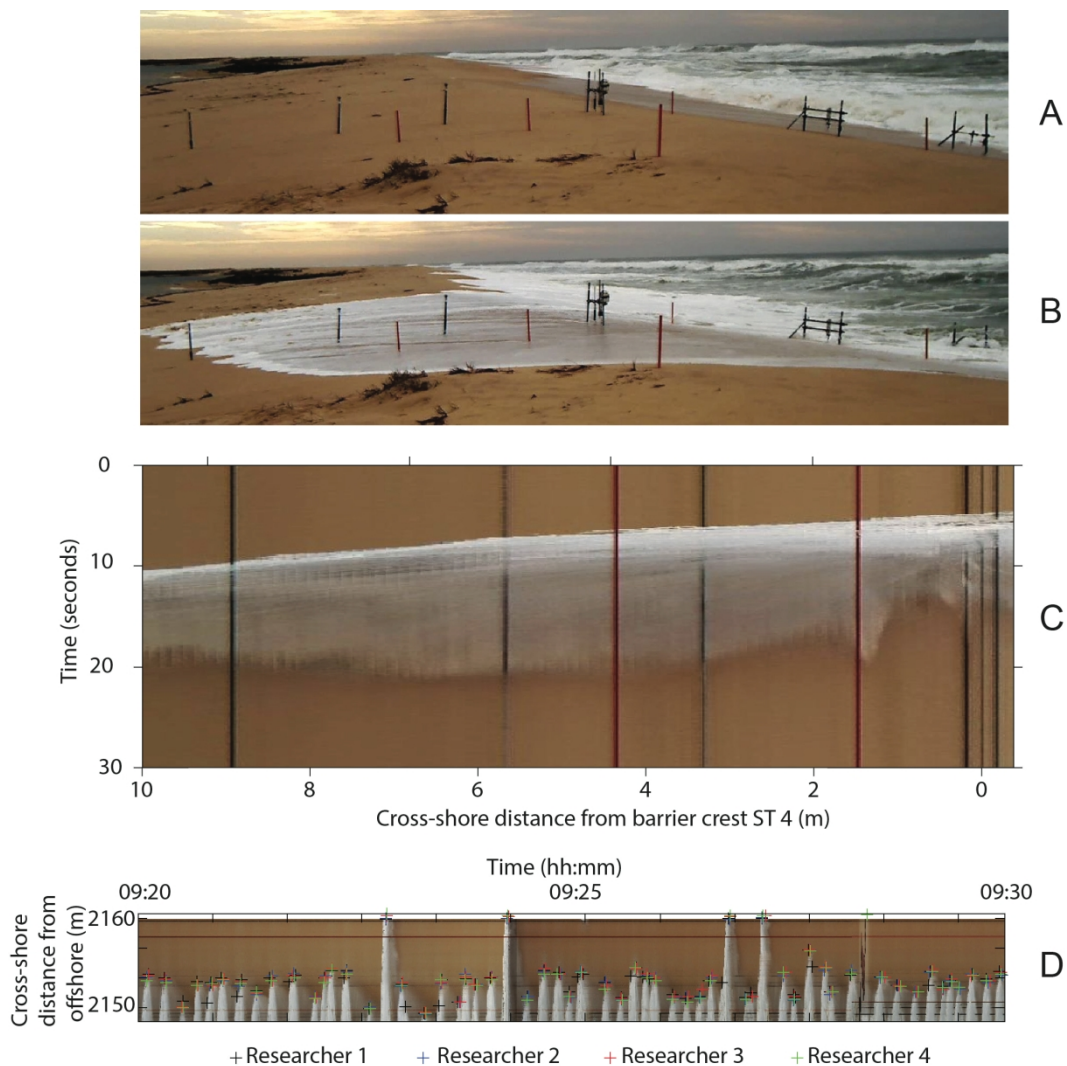
244 Image frames were extracted from the video at the same acquisition frequency (i.e.  
245 10Hz) resulting on approximately 170000 images (1600x1200 pixel resolution).  
246 The camera intrinsic parameters were determined with the Camera Calibration  
247 Toolbox of Bouguet (2007) to correct lens-induced distortions on the images.  
248 Overwash Timestack images were produced sampling the pixel array (0.1 m spatial  
249 resolution) located along the instrumented barrier profile over the image sequence,  
250 and considering sampling periods of 10 minutes (Figure 3 as an example). On the  
251 Timestacks images the overwash water front was visible as white stripe line, which  
252 was automatically detected based on pixel intensity variation. The average leading-  
253 edge velocity of each overwash event on the barrier was estimated through the  
254 intersection of the detected water line with instruments' positions, and Timestack-  
255 based leading edge velocity was compared to flow velocity obtained with the current  
256 meter.

257 Runup Timestack images were generated between low tide water level and the  
258 barrier crest positions during the 3.5 hours of video acquisition. To extract the  
259 runup elevation for each swash event, the maximum of the visual edge of the water  
260 excursion was manually digitized, on each of the georeferenced 22 Timestack  
261 images/datasets. The cross-shore distances (swash) were then converted into  
262 elevations (runup referred to MSL), using the interpolated barrier profiles  
263 corresponding to each 10-min Timestack images with 0.1 m cross-shore resolution  
264 (following procedures that can be found e.g. in Vousdoukas et al., 2011; Blenkinsopp  
265 et al., 2015; Andriolo et al., 2018). Number of runup values varied between a  
266 minimum of 45 to a maximum of 60 values per Timestack over the dataset. Because  
267 there is a certain degree of subjectivity in the manual digitizing of runup, an analysis  
268 of operator variability was made. Four experienced coastal researchers were asked  
269 to independently mark the maximum swash of all events, on the 22 Timestack image  
270 datasets (Figure 3, as an example). The Kruskal-Wallis test was used to test the  
271 hypothesis that the runup results obtained by the several operators were  
272 significantly different. The test indicated that there is a 95% probability that the  
273 results obtained by the operators are not statistically different. Based on average  
274 results of runup obtained by the four operators, the 2% exceedance runup ( $R_2$ ), the  
275 10% exceedance runup ( $R_{10}$ ) and the significant runup ( $R_{sig}$ , the average of the top  
276 third of runup values) were calculated. The runup statistics were computed  
277 assuming a normal distribution fit, which was found to consistently represent runup  
278 distribution by similar previous works (e.g., Stockdon et al., 2006; Hughes et al.,  
279 2010; Atkinson et al., 2017).

280 In summary, across the beach face only runup measurements were obtained from  
281 Timestack imagery; at the barrier crest overwash depth was recorded by a PT and

282 the velocity obtained from electromagnetic current meter and from Timestack  
 283 imagery; and at the barrier top, the overwash water intrusion distance was  
 284 extracted from Timestack images also. This substantial reduction from the initial  
 285 seven field stations was related to the intense erosion on the beach face, which led  
 286 to the collapse of the supporting structures fall and subsequent loss of equipment,  
 287 to equipment damage when exposed to the turbulent swash zone, and the  
 288 impossibility of manual measurements of bed variations (for example on rods) on  
 289 stations 5, 6 and 7 due to the high frequency of overwash during high-tide (about 1  
 290 event per minute).

291



292

293 **Figure 3 – A and B. Undistorted and cropped images obtained from post-processing video imagery at**  
294 **two timings of an overwash event. C. Timestack with an overwash event produced over 30 seconds.**  
295 **Stations are visible as black vertical lines (ST4 at the crest, on the right, is represented by three black**  
296 **lines, one for each pole and one for the CM) and control points as red lines (red poles). C. Example of**  
297 **runup marking by different researchers on a 10-min Timestack.**

298

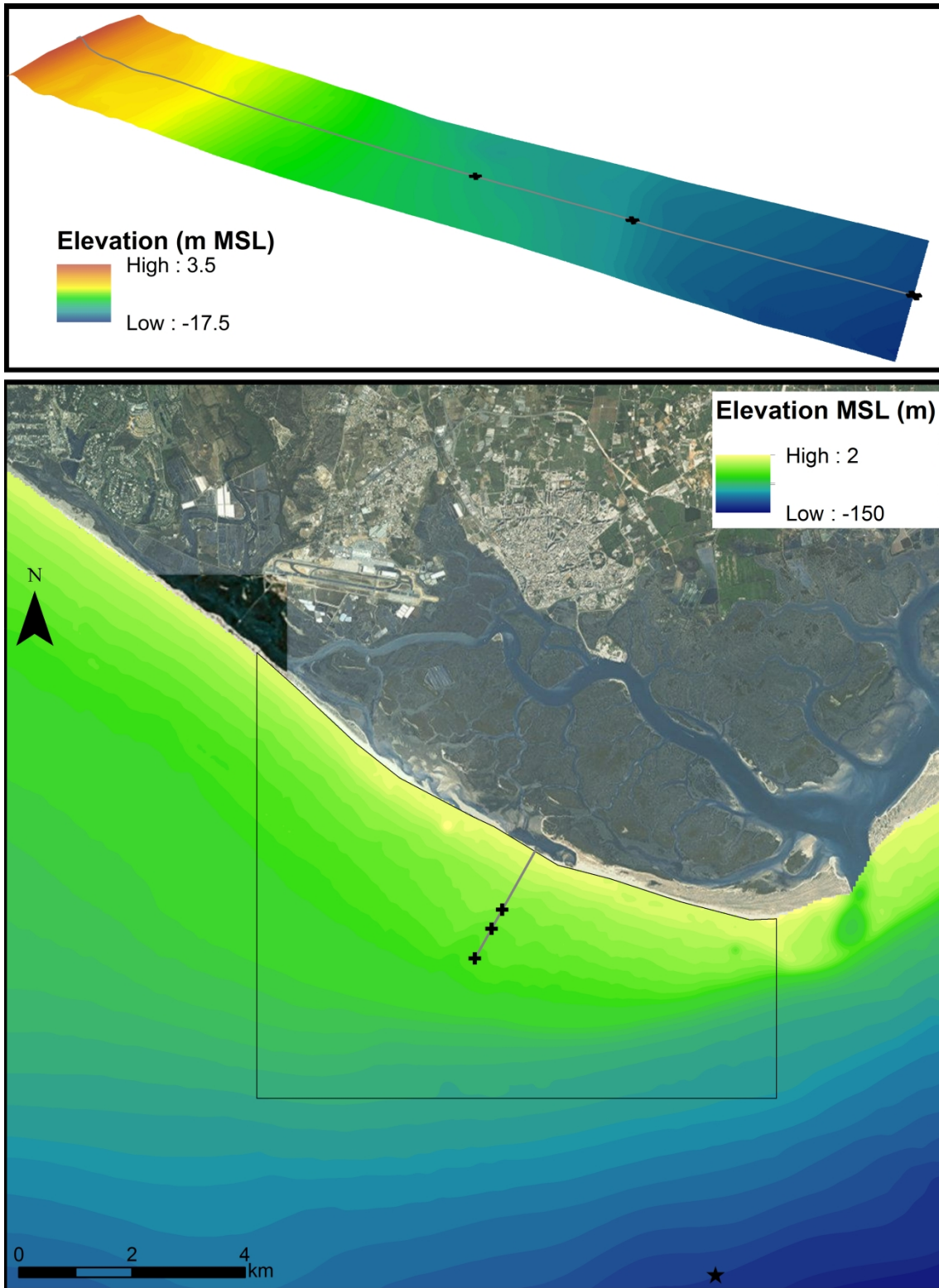
299

### 300 **3.3. TOPOGRAPHY, BATHYMETRY AND GRAIN-SIZE**

301 Barrier morphology was measured before (at 5:30) and after (at 13:00) the  
302 overwash episode (from 08:40 to 12:20) using an RTK-DGPS. Cross-shore profiles  
303 during the overwash event were impossible to obtain, therefore profiles were  
304 interpolated from the initial and final profiles. Topographic bed changes for each 10-  
305 min were obtained by weighting the overall bed change by the percentage of  
306 overwash events that occurred during each 10-min.

307 Offshore bathymetry of the inner-shelf of the study area, from the shoreline to  
308 depths of approximately MSL-25 m and extending for about 5 km roughly centred  
309 in the fieldwork site, was collected using a survey-grade single beam echo sounder  
310 (Odom Ecotrac CV100). Precise positioning and real-time tide correction were  
311 obtained using an RTK-DGPS and all data were synchronized and processed with  
312 Hypack software (further details on the acquisition system are provided in Horta et  
313 al., 2014). Bathymetric surveys were performed on multiple occasions from June  
314 2012 to April 2013, including both pre and post-overwash conditions. Data from the  
315 dedicated surveys were combined with offshore bathymetric data provided by the  
316 Hydrographic Institute of Portugal to create a bathymetric grid extending from the  
317 shoreline to the location of the Faro offshore wave buoy (Figure 4). Bathymetric  
318 grids were produced in Surfer software, using Kriging interpolation and considering

319 a linear semi-variogram model. Additionally, cross-shore profiles to be used as input  
320 on the XBeach model were interpolated for a 500 m-wide section centred on the  
321 fieldwork site and extending, in the cross-shore dimension, for more than 2,000 m  
322 from the backbarrier to a depth of MSL -15 m.



323

324 Figure 4 – Location and bathymetry of grids used in wave modelling. Upper panel - high-resolution  
 325 grid of the cross-shore section centered on the fieldwork site profile (grey line), with locations of  
 326 depths MSL-12, -15 and -17 m (black crosses) for reference. Lower panel - bathymetry of the 50m-  
 327 resolution regional grid, with extent of the 20 m-resolution nested local grid (black polygon). Black  
 328 star indicates the location of the offshore directional wave buoy.

329

330 Surficial sediment samples were collected at all stations after the overwash episode.  
331 Samples were analysed using traditional laboratory dry sieving procedures for  
332 unconsolidated clastic sediments. Sieving was done for sediment grain-sizes  
333 between 31.5 mm and 0.063 mm. Percentiles  $D_{10}$ ,  $D_{50}$  (median), and  $D_{90}$  were  
334 determined using GRADISTAT (Blott and Pye, 2001). Sediment porosity was  
335 determined in the laboratory from the void volume ratio of samples.

336 Further information on the study site grain-size variability was obtained from  
337 previous measurements on beaches, dunes and washovers near the study area  
338 described in Matias et al. (2009). Information of the nearshore sediment grain-size  
339 was obtained from a systematic study of sediments from the inner shelf of the Ria  
340 Formosa barrier system published in Rosa et al. (2013).

341

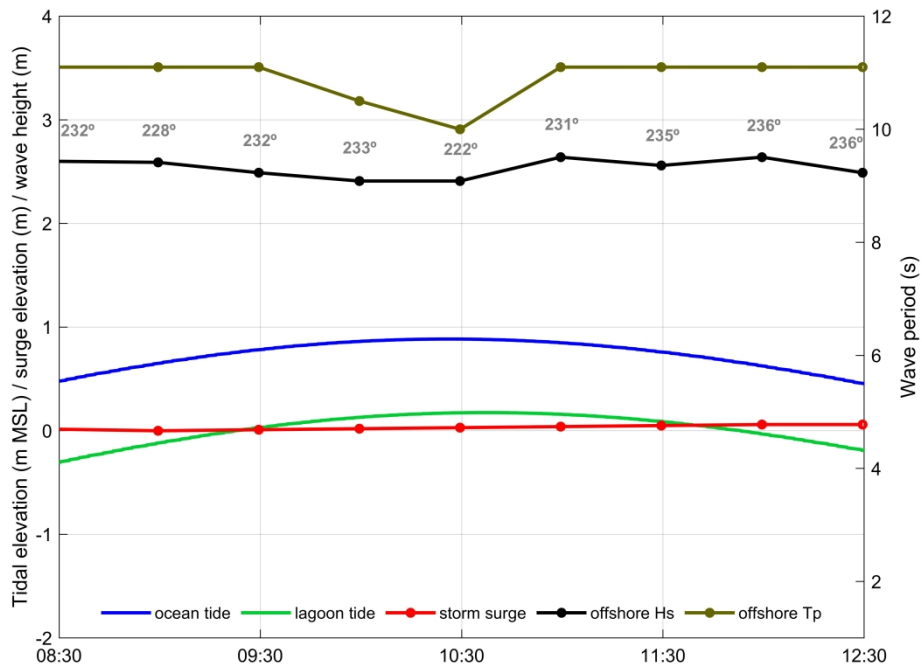
342

## 343 **4. FIELDWORK RESULTS**

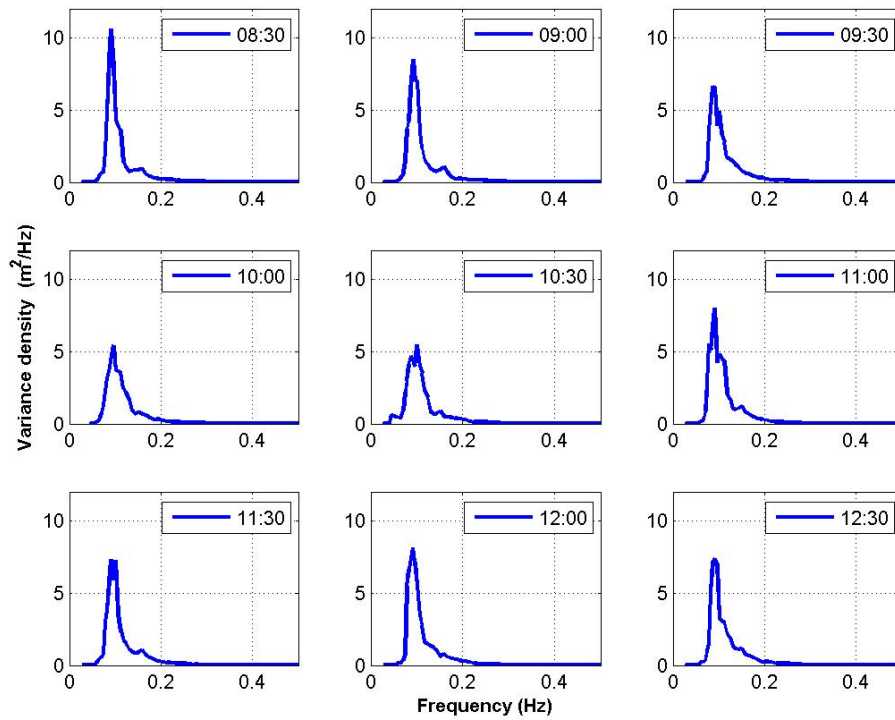
344

### 345 **4.1. HYDRODYNAMICS**

346 During the fieldwork campaign, which occurred during neap tides, tidal levels  
347 reached a maximum of about MSL +0.9 m on the ocean side, between 10:00 and  
348 10:30, whilst lagoon tidal elevations varied between 0.17 m and -0.3 m MSL (Figure  
349 5A). Storm surge was almost insignificant, ranging between 0.00 m and 0.06 m.  
350 Offshore waves measured by the Waverider buoy averaged 2.5 m, with the highest  
351  $H_s$  of 2.64 m recorded at 11:00 (close but not exceeding the storm threshold for this  
352 area, 3.0 m).



353



354

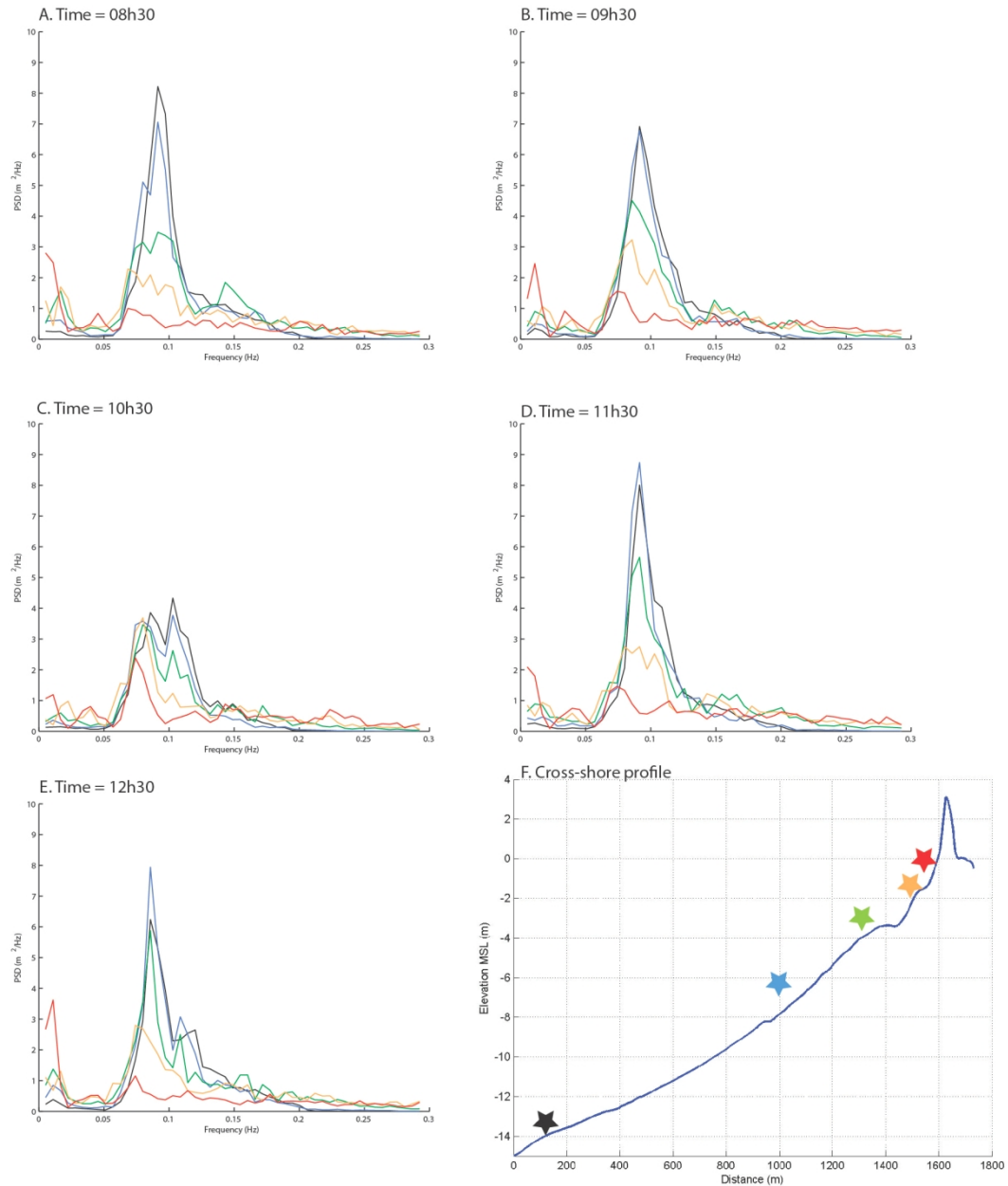
355 Figure 5 – A. Synthesis of oceanographic conditions during the overwash episode on 12/12/2013. B.  
 356 Modelled nearshore wave spectra at a depth of MSL-15 m.

357

358

359 At about MSL-12 m depth, wave refraction and bed friction had reduced  $H_s$  to 2.0 m  
360 – 2.2 m. Waves approached mainly from a SW direction, with an offshore incident  
361 angle always smaller than 30 degrees, and a nearshore angle smaller than 12  
362 degrees. During most of the overwash episode, wave spectra were relatively broad  
363 in frequency, slightly narrower at the beginning (8:30; Figure 5B and 6A). The  
364 highest wave energy peak was associated with wave frequencies around 0.09 Hz,  
365 with a second mode around 0.11 Hz. Although several and variable peaks in wave  
366 spectra were recorded offshore, two main sets of waves could be identified on the  
367 SWAN model output at the MSL-15 m depth. The bi-modal shape of most of the  
368 modelled wave spectra, indicates the combination of two wave fields and curve-  
369 fitting with various JONSWAP spectra suggests that these two wave fields are  
370 characterised by  $H_s = 2$  m and  $T_p$  of 11.3 s, and  $H_s = 1.3$  m and  $T_p$  of 8.8 s.

371

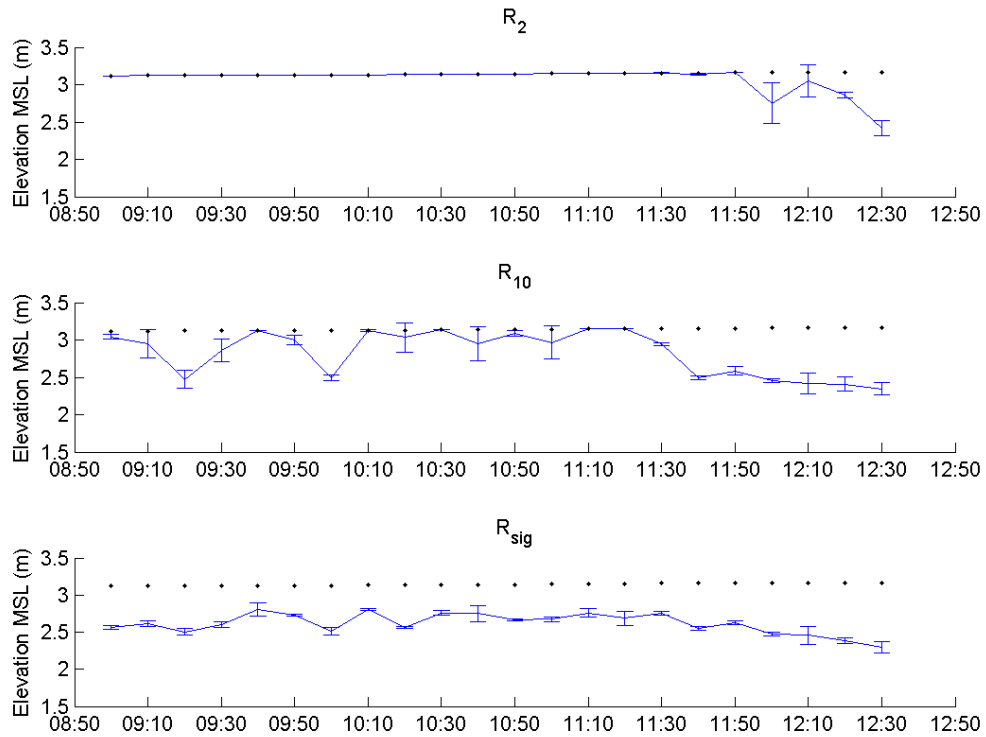


372  
 373 **Figure 6 – Example of the transformation of the wave spectra modelled across the offshore and**  
 374 **nearshore profile for several time-steps (08h30, 09h30, 10h30, 11h30 and 12h30, for panels A to E,**  
 375 **respectively). Stars on the cross-shore profile (panel F) represent the location where the spectra**  
 376 **were extracted, and star colours corresponds to line colour of spectra represented in panels A to E.**

377

378 Runup elevation during the overwash episode is a main parameter controlling the  
 379 variation and number of overwash events. At the peak of high-tide (10:30) runup  
 380 parameters  $R_2$  and  $R_{10}$  are identical (Figure 7) and coincide with the level of the  
 381 barrier crest.  $R_{\text{sig}}$  is more variable but still dominantly influenced by overwash;

382 values do not increase significantly during high-tide because swash up-slope motion  
 383 is limited.



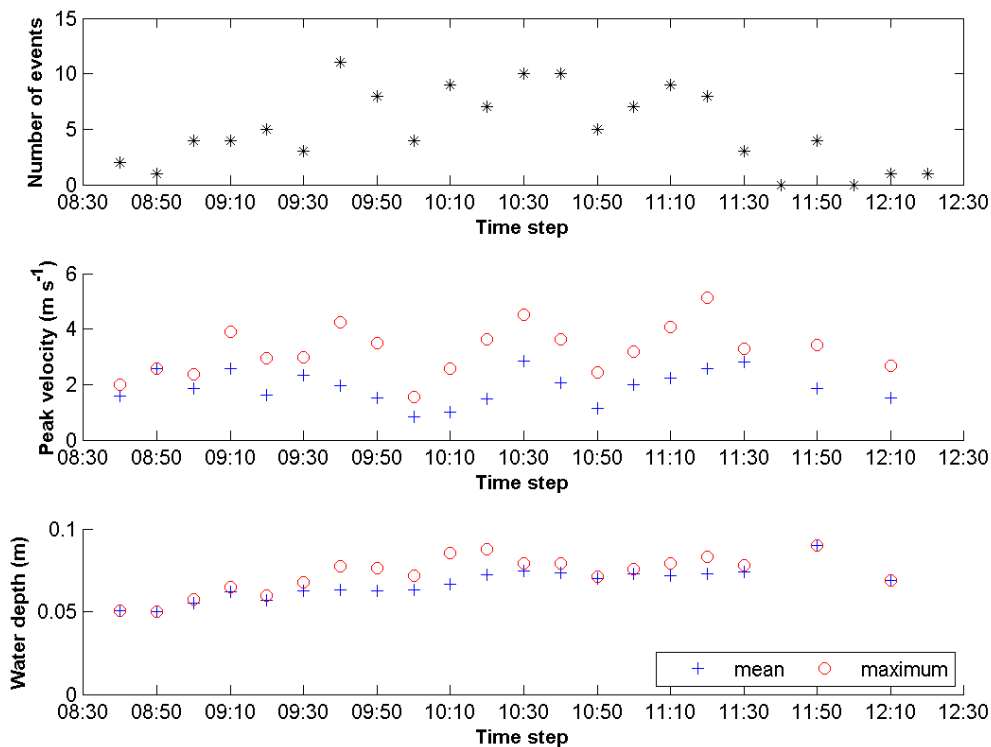
384

385 **Figure 7 – Statistics of runoff during the entire overwash episode.  $R_2$  is the 2% exceedance of runoff,**  
 386  **$R_{10}$  is the 10% exceedance runoff and  $R_{sig}$  is the significant runoff (i.e.,). The barrier crest elevation**  
 387 **is represented by the black dots. The error bars are the standard deviation of each 10-min runoff**  
 388 **measurement, considering the results from four operators.**

389

390 During the surveyed overwash episode a number of overwash events, defined as a  
 391 single passage of water above the barrier crest, occurred. For more than 4 hours,  
 392 circa 120 overwash events occurred over the barrier crest were measured at the  
 393 instrumented cross-shore profile. About 70% of these overwash events occurred  
 394 between 09:45 and 11:45 (Figure 8). Most overwash events had limited inland  
 395 intrusion ( $< 2$  m) beyond the crest of the barrier; yet, some events reached the  
 396 backbarrier lagoon. Peak overwash flow velocity was generally between 1 and 3 m s<sup>-1</sup>

397 <sup>1</sup>, although maximum velocities reached values close to 5 m s<sup>-1</sup> (maximum 5.1 m s<sup>-1</sup>  
 398 measurement by the current meter and 4.7 m s<sup>-1</sup> from video imagery) Average  
 399 overwash leading edge velocity obtained with video imagery was 2.1 ms<sup>-1</sup>, similar  
 400 to the average overwash velocity 1.9 ms<sup>-1</sup> measured by EM current meter. Overwash  
 401 flow was very shallow (Figure 8), with mean depth of 0.07 m. These characteristics  
 402 are typical of overwash flows, which are generally supercritical (according to data  
 403 compiled by Matias and Masselink, 2017). Larger overwash events had deeper and  
 404 faster flows, as well as longer durations and larger intrusion distances. Despite the  
 405 reduction in number of events at the start and end of the fieldwork campaign and  
 406 variable peak velocities, depths of overwash flows were relatively constant (Figure  
 407 8).



408

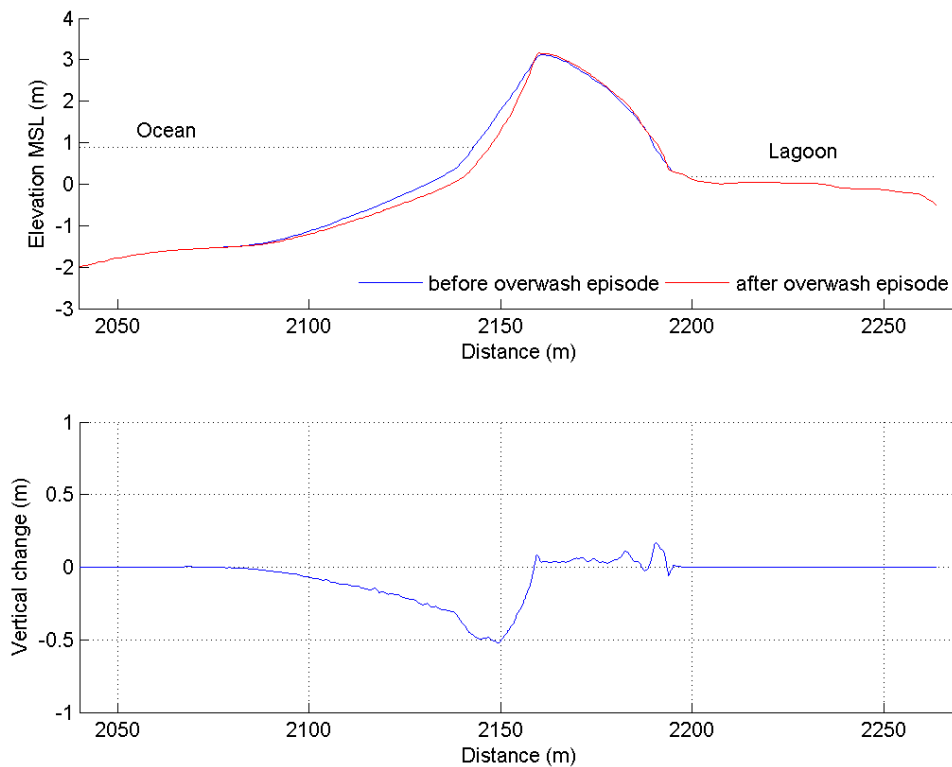
409 **Figure 8 – Overwash events average properties during the entire overwash episode, obtained from**  
 410 **the video Timestacks (velocity) and PT (depth) at ST 4 (see Figure 2 for location).**

411

412 **4.2. MORPHOLOGY AND GRAIN-SIZE**

413 During the overwash episode, the beach face was eroded and sand accumulated on  
414 the barrier top and farther inland across the barrier (Figure 9). The beach face is  
415 steep (average slope of 0.1), with average beach  $D_{50}$  (median grain-size) of 0.61 mm  
416 (Table 1). The backbarrier surface facing the lagoon has variable slope, exhibiting a  
417 coarsening grain-size and a poorer sorting due to the presence of overwash debris  
418 lines. Barrier porosity is mostly around 0.3 with a maximum of 0.36 close to ST7  
419 (location on Figure 2). According to data from Matias et al. (2009), at the western  
420 part of Barreta Island the average beach  $D_{50}$  is 0.65 mm, varying between 0.47 mm  
421 and 0.89 mm. In the nearshore area, the average  $D_{50}$  is 0.36 mm, whilst offshore  
422 sediments became coarser (average  $D_{50} = 0.43$  mm, according to Rosa et al., 2013).

423



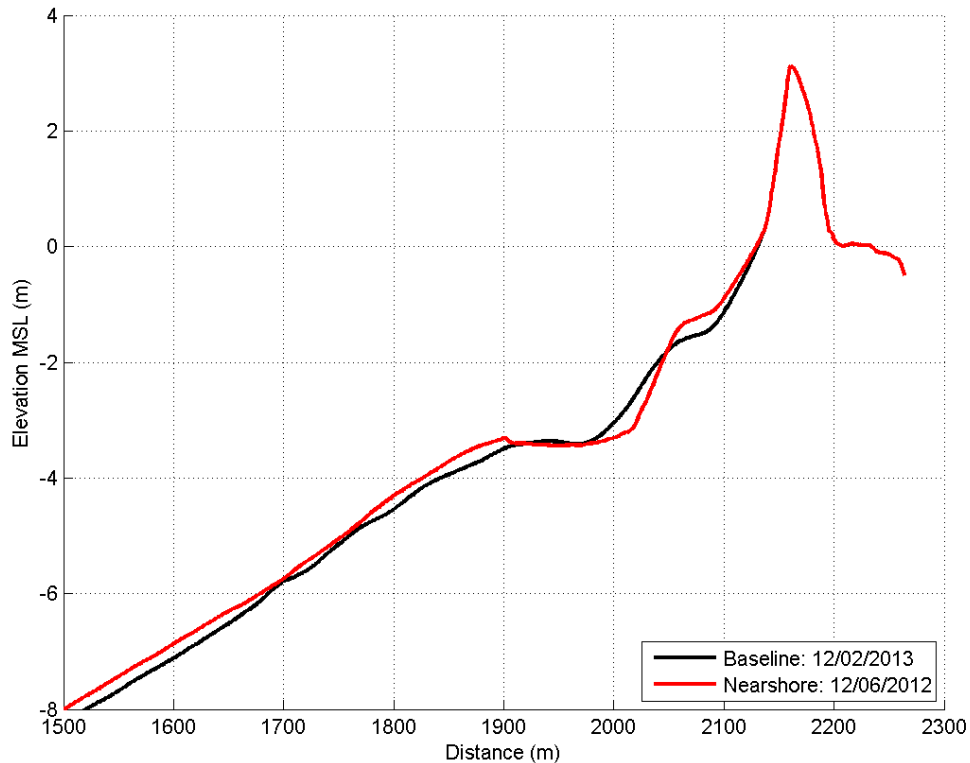
424

425 **Figure 9 – Topographic profiles of the barrier before and after the overwash episode. The dashed line**  
 426 **represents the maximum ocean and lagoon tidal levels. On the lower panel are represented the**  
 427 **morphologic variations across the barrier profile during the overwash episode.**

428

429 Observed changes indicate that the volume of barrier erosion was greater than the  
 430 volume of overwash induced deposition. The net sediment balance is  $-13.7 \text{ m}^3\text{m}^{-1}$ ,  
 431 with only about  $1.8 \text{ m}^3\text{m}^{-1}$  of overwash deposition on the barrier. The net loss of  
 432 sediment is either attributed to longshore sediment transport or offshore sediment  
 433 transport to areas below the topographic survey. The topography at the end of the  
 434 overwash episode was only surveyed down to MSL -1 m on the ocean margin; below  
 435 this depth, a former nearshore survey was used to reconstruct the barrier  
 436 morphology. The nearshore area, between MSL -1 m and -3.5 m typically exhibits a  
 437 sandbar that changes in morphology and elevation through time (Figure 10). It is

438 possible that cross-shore sediment transport during this event while contributing  
439 to sandbar formation, led to offshore sediment loss from the barrier.



440

441 **Figure 10 – Profiles with different nearshore morphologies. The subaerial section was measured**  
442 **after the overwash episode, while the nearshore section was measured in February 2013 (labelled**  
443 **Baseline, with the date closest to the overwash episode). The nearshore section was also measured**  
444 **in other occasions, with profile Nearshore displaying the June 2012 morphology.**

445

446

## 447 5. HYDRODYNAMIC MODELLING

448

### 449 5.1. MODEL SET-UP: Barreta baseline overwash model

450 This study uses the one-dimensional approach of XBeach model developed by  
451 Roelvink et al. (2009). XBeach is a process-based hydrodynamic and

452 morphodynamic model developed to assess the natural coastal response to time-  
 453 varying storm and hurricane conditions. In this study the model was run in non-  
 454 hydrostatic (wave-resolving) mode (Smit et al., 2012; McCall et al., 2014), including  
 455 groundwater processes (McCall et al., 2012; McCall et al., 2014), but without the  
 456 computation of morphological changes. Model setup consisted of three stages:  
 457 definition of boundary forcing conditions, generation of the model grid and  
 458 parametric adjustments. The boundary forcing conditions were defined using field  
 459 data, when available, or from modelled outputs. Variables used as boundary  
 460 conditions include: barrier profile (Figures 9 and 10), modelled wave spectra at  
 461 depths of MSL-12 m, -15 m and -17 m (details in section 3.1) (Figure 5B), ocean and  
 462 lagoon water levels (Figure 5A), and  $D_{50}$  (Table 1), whilst other non-measured  
 463 parameters were kept at their default values (e.g., bed friction). The hydraulic  
 464 conductivity (K) was computed with Hazen's equation (Table 1), using measured  
 465  $D_{10}$ . The generated grid is non-equidistant, with a minimum grid size of 0.1 m  
 466 onshore and a maximum grid size of 3 m offshore, observing the limiting condition  
 467 of a minimum of 50 points per wavelength (Table 1).

468

469 **Table 1 – Input parameters for XBeach model.**

| Parameter                     |                                |
|-------------------------------|--------------------------------|
| Minimum grid size (m)         | 0.1                            |
| Maximum grid size (m)         | 3                              |
| Minimum points per wavelength | 50                             |
| Offshore boundary             | Z = -15 m                      |
| Duration (s)                  | 2340 ; including 600 s spin-up |
| Output timestep (s)           | 0.25                           |
| $D_{50}$ (m)                  | 0.00061                        |
| K ( $\text{ms}^{-1}$ )        | 0.0015                         |

470

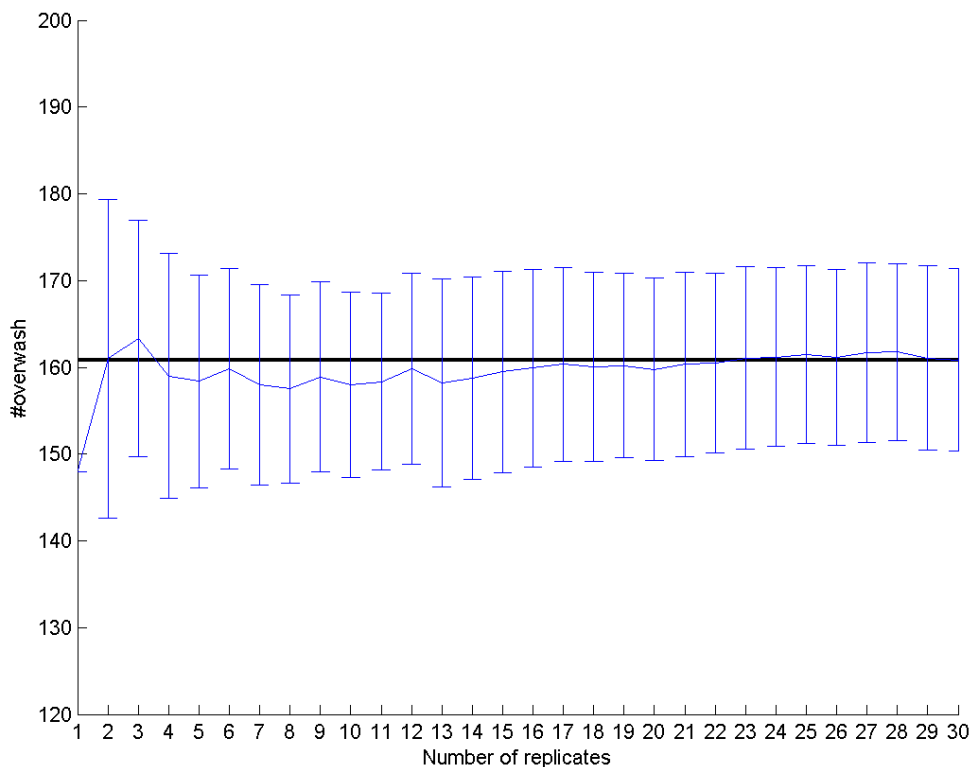
471 Validation of the model is achieved by comparison of observed and modelled wave  
472 runup and overwash statistics. While no observed nearshore spectral wave data  
473 were available for a quantitative validation of the nearshore wave height, Figure 6  
474 does qualitatively illustrate the changes in the modelled wave spectra across the  
475 nearshore profile during the overwash episode. Wave energy decreased as waves  
476 propagated into the nearshore, with the most significant transformations occurring  
477 between depths of MSL -4 m and the shoreline. As depth decreases and waves  
478 propagate landward of the nearshore bar there was an increase in wave energy on  
479 the infra-gravity band and the widening of the spectra, particularly noticeable for  
480 narrow offshore spectra conditions (e.g., Figure 6 A and 6D).

481 Further XBeach setup adjustments were carried out on the offshore boundary, spin-  
482 up duration and number of replicates. The offshore extent and depth at the offshore  
483 boundary of the XBeach model was decided by balancing two opposite criteria: (i)  
484 the boundary should be located in relatively deep water to correctly account for  
485 infragravity wave energy associated with long-period incident-band waves; and (ii)  
486 it should be located in water shallow enough to account for most of wave refraction  
487 and to minimize dispersion errors related to the numerical scheme of the model.  
488 Considering the wave conditions measured during the overwash episode and a ratio  
489 between wave group velocity and phase velocity  $< 0.85$  (Deltares, 2014), a  
490 boundary at depths bellow MSL-17 m would be preferable. However, as waves at  
491 this depth were not yet shore-normal ( $12^\circ - 26^\circ$  relative to shore-normal) and  
492 refraction cannot be accounted for in a 1D model, as a compromise, the offshore  
493 boundary was set in an intermediate location, at MSL -15 m. For XBeach, the offshore  
494 boundary was set at  $x = 0$  m and  $z = -15$  m (Table 1), and the domain, represented

495 in Figure 4, has a cross-shore extension of 1730 m. XBeach in non-hydrostatic mode  
496 is a phase-resolving model; therefore, at the start of each run waves propagating  
497 across the nearshore do not reach the barrier, and the groundwater surface needs  
498 time to adjust. Runs were made with an initial time (the 'spin-up') of 10, 20 and 30  
499 minutes durations. It was concluded that a spin-up of 10 minutes provided good  
500 results whilst maintaining a reasonable computational effort.

501 Since the XBeach model simulates hydrodynamics based on a random realisation of  
502 the imposed wave-spectra, which are statistical quantities obtained over 30-  
503 minutes, model results may vary between simulations with the same statistical  
504 boundary conditions, but different random realisations of the wave field. Figure 11  
505 shows the variation in the average number of overwash events with an increase in  
506 the number of replicates. Replicates in this context are model runs of the nine 30-  
507 minutes time-steps, with exactly the same input conditions (e.g., grain-size, grid size,  
508 tide elevation, spectra parameters). For each replicate, an overall number of  
509 overwash events was obtained (270 minutes duration of the overwash episode). A  
510 power analysis was performed to estimate the number of replicates (sample size)  
511 needed to allow accurate and reliable statistical evaluation. In this context, power  
512 analysis serves to estimate the number of modelling replicates needed to have a  
513 good chance of detecting overwash differences between different tests that are not  
514 due to differences in random realisations of the wave field. To conduct the power  
515 analysis, it was necessary to set a number of variables: mean and standard deviation  
516 of number of overwash events, effect size, and power. The effect size is the minimum  
517 deviation that needs to be detected, while power is the probability of distinguishing  
518 a minimum effect. An effect size of 10% and a power of 95% were decided based on  
519 the literature (e.g. McDonald, 2014), and assured a very high chance of observing an

520 effect that is real. A mean number of 160 overwash events and a standard deviation  
 521 of 10 were used (Figure 11) for power computation. The obtained number of  
 522 replicates was 6. The overwash episode was divided into 9 time steps of 30 minutes  
 523 (with 10 minutes spin-up), from 08:30 to 12:30. The output time-step was set at 4  
 524 Hz, matching the sampling grid of the instruments.



525

526 **Figure 11 – Average and standard deviation of overwash number of events for the entire episode**  
 527 **considering an increasing number of replicates. The coarser black line is the overwash number of**  
 528 **events after 30 replicates (161 events).**

529

## 530 5.2. BASELINE MODEL PERFORMANCE

531 The performance and evaluation of model usefulness as a predictive tool was  
 532 assessed using standard metrics of performance, particularly bias (eq. 1), root-  
 533 mean-square error (RMSE, eq. 2), and scatter index (SCI, eq. 3), as described in

534 McCall et al. (2014). The model overwash statistics for each 30-minute period  $i$   
 535 ( $x_{i,modelled}$ ), were compared against overwash statistics computed from field data for  
 536 the same duration ( $x_{i,measured}$ ). The mean error describes the potential bias as  
 537 follows:

$$538 \text{ Bias}(x) = \frac{1}{N} \sum_{i=1}^N (x_{i,modelled} - x_{i,measured}) \quad (1)$$

539 Where  $N$  is the number of time-steps (9 for this particular case). The RMSE  
 540 measures the difference between values predicted by a model and the values  
 541 actually observed from the environment that is being modelled, and is defined as  
 542 follows:

$$543 \text{ RMSE}(x) = \sqrt{\frac{1}{N} \sum_{i=1}^N (x_{i,modelled} - x_{i,measured})^2} \quad (2)$$

544 SCI is a relative measure of the scatter between model and data as follows:

$$545 \text{ SCI}(x) = \frac{\text{RMSE}(x)}{\max\left(\frac{1}{N} \sum_{i=1}^N x_{i,measured}, \sqrt{\frac{1}{N} \sum_{i=1}^N x_{i,measured}^2}\right)} \quad (3)$$

546 The error is normalized with the maximum RMSE of data and the absolute value of  
 547 the data mean to avoid anomalous results for data with small mean and large  
 548 variability. Bias, RMSE and SCI closest to zero represent better model performances.  
 549 The model performance metrics are presented in Table 2. Results indicate that the  
 550 model overestimates the number of overwash events; for all time-steps an average  
 551 of 5 additional overwash events are produced by the model, which represents an  
 552 overestimation of approximately 25 %. The baseline model performance changes  
 553 throughout the event; during the rising tide the baseline model under- or over-  
 554 predicts by only 2-4 events, while during the falling tide the baseline model over-  
 555 predicts overwash by 4-14 events.

556

557 **Table 2 – Summary of performance metrics of baseline model according to average number, depth**  
558 **and velocity of overwash events. Values are averages for all time-steps.**

| Parameter                                  | Model performance |      |      |
|--|-------------------|------|------|
|  | Bias              | RMSE | SCI  |
| Number of overwash events                  | 5                 | 7    | 0.27 |
| Peak overwash depth (m)                    | 0.02              | 0.02 | 0.30 |
| Peak overwash velocity (ms <sup>-1</sup> ) | 0.43              | 0.61 | 0.28 |

559

560 Overwash depth and velocity are also overestimated by about 20%; however, these  
561 values are very small (0.02 m and 0.4 ms<sup>-1</sup>) and within the error margin of the  
562 measurements under the demanding fieldwork conditions. The SCI for the number,  
563 depth and velocity of overwash events is consistently low to moderate (c. 0.3).

564 The comparison between the fieldwork runup statistics and the modelled runup  
565 statistics is also an indicator of the model performance. The average difference  
566 between the field  $R_{sig}$  and the model  $R_{sig}$  each 10 minutes is 0.2 m, with the model  
567 overestimating conditions measured in the field. Because overwash flows are so  
568 shallow, a 0.2-m difference in significant runup represents an increase of 25% of  
569 overwash events over the crest, which may be due to overestimation of offshore  
570 water level or wave swash computations.

571

### 572 **5.3. BASELINE MODEL VERIFICATION**

573 In order to verify that the Barreta baseline overwash model consistently provides  
574 reasonable predictions of overwash, the model was applied to other situations when  
575 overwash was measured in the same profile, at Barreta Island, during the period  
576 referred previously (June 2012 to April 2013). Field surveys, including topography

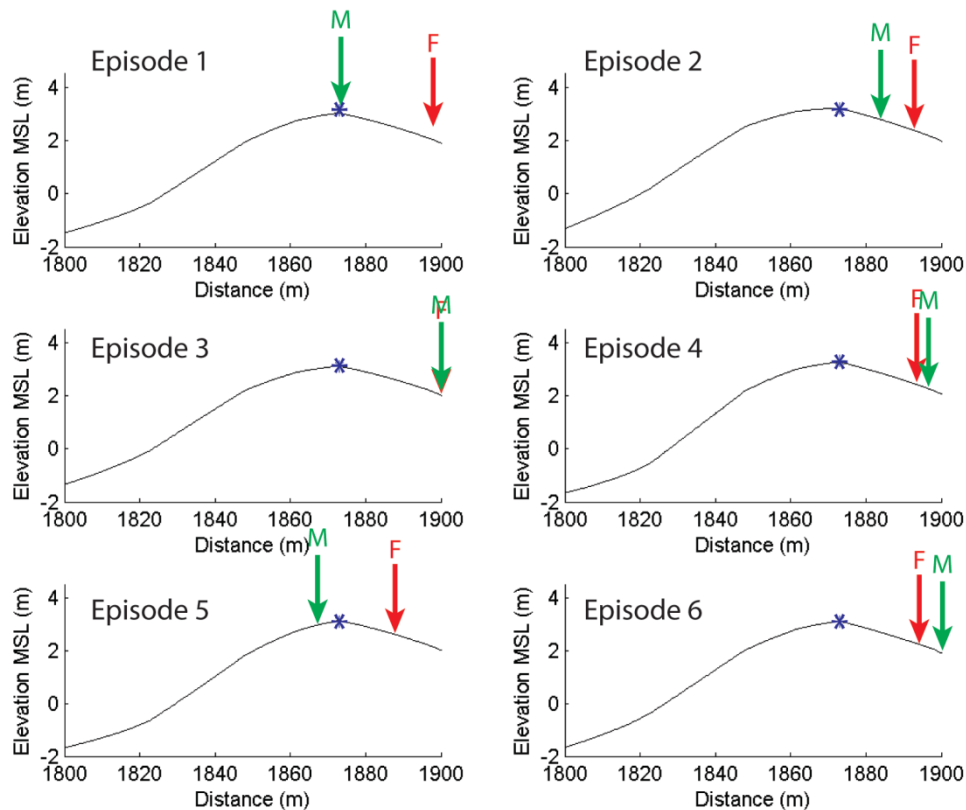
577 and bathymetry, were undertaken before and after each of six overwash episodes,  
 578 although no instrumentation was deployed on the barrier and thus there were no  
 579 measurements of runup or overwash hydrodynamics. For the post-overwash  
 580 episode surveys, the maximum overwash intrusion on the barrier island top was  
 581 surveyed in detail with RTK-DGPS (for further details about this dataset refer Matias  
 582 et al., 2014). Measured offshore waves for the overwash episodes were used to force  
 583 nearshore wave propagation as described for the calibration fieldwork (section 3.1).  
 584 The six post-overwash topo-bathymetric surveys, named for simplicity as “Episode  
 585 1” to “Episode 6” characteristics can be found in Table 3. Episode 1 to Episode 6  
 586 characteristics (morphology, waves, maximum tide level) were used as inputs to the  
 587 calibrated baseline model, while other parameters remained unaltered. For each  
 588 modelled overwash episode, the location of the maximum water intrusion on top of  
 589 the barrier was extracted and compared with fieldwork (Figure 12).

590

591 **Table 3 – Conditions of the six overwash episodes verification cases**

|           | Date       | Hs   | Tp   | Tide |
|-----------|------------|------|------|------|
| Episode 1 | 02/10/2012 | 0.73 | 9.1  | 1.35 |
| Episode 2 | 31/10/2012 | 2.15 | 9.4  | 1.31 |
| Episode 3 | 19/11/2012 | 2.01 | 8.6  | 1.92 |
| Episode 4 | 31/01/2013 | 1.02 | 12.5 | 1.36 |
| Episode 5 | 13/02/2013 | 0.79 | 9.4  | 1.51 |
| Episode 6 | 13/03/2013 | 1.40 | 9.41 | 1.80 |

592



593 M - model max intrusion F - field max intrusion \* barrier crest location

594 **Figure 12 – Maximum overwash water intrusion over the barrier crest obtained during fieldwork**  
 595 **measurements and after modelling results.**

596

597 Results show that the modelled and measured maximum water intrusion have  
 598 relatively good agreement, although not always coincident (average horizontal  
 599 difference = 8.6 m and average vertical difference = 0.2 m). Minimum difference in  
 600 overwash water intrusion across the barrier is close to zero (Episode 4, Figure 12)  
 601 and maximum difference was observed for Episode 1, where fieldwork  
 602 measurements show a maximum swash excursion of 56.5 m from the average water  
 603 line position, thus causing significant overwash and the model estimated a swash  
 604 excursion of 31.5 m. During Episode 5, the model failed to predict overwash  
 605 occurrence, although by a small amount (Figure 12). This result is somewhat  
 606 unexpected since the results of the calibration have shown that the model over-

607 predicts overwash by 20 to 25%. Limitations in correctly identifying the line of  
608 maximum intrusion of a specific episode, in an area where overwash occurs  
609 frequently, may be one cause of this mismatch, alongside errors in model boundary  
610 conditions such as the (dynamic) submarine and subaerial barrier profile (see e.g.,  
611 Section 6.2). When possible, fieldwork was undertaken only a few hours after  
612 overwash, when the overwash debris line was coincident with a wet/dry sand line.  
613 However, in case of Episode 1 such an early survey was unfeasible due to technical  
614 constraints and it is possible that the marked debris line (marked F in Figure 12)  
615 may corresponded to a previous overwash episode.

616 Overall, the Barreta baseline overwash model performs fairly well in predicting  
617 hydrodynamics in the study area, because the BIAS, RMSE and SCI are relatively  
618 small, and the verification episodes are also generally well simulated.

619

## 620 **6. MODELLING ANALYSIS**

621 The Barreta baseline overwash model was further explored to analyse the relative  
622 importance of several factors in overwash occurrence, namely: (1) hydrodynamic  
623 parameters, particularly waves and lagoon water levels; and (2) nearshore  
624 morphological configurations of the barrier and barrier grain-size. To evaluate the  
625 contribution of these factors, the Barreta baseline overwash model was changed in  
626 only one parameter at a time, keeping the remaining unaltered. Each modified  
627 model was also replicated six times (see section 5.1) and ensemble-mean results are  
628 presented. The output variables (runup, number of overwash events, overwash  
629 depth, velocity and discharge) were compared with the baseline model, aiming to  
630 understand their relative importance in overwash processes.

## 632 6.1. HYDRODYNAMIC PARAMETERS

633 The wave conditions used to setup and verify the Barreta overwash model have an  
 634 annual probability of occurrence of about 50%, for waves from W and SW.  
 635 (according to data described in Costa et al., 2001). To observe how much overwash  
 636 hydrodynamic parameters change under more extreme (less frequent) conditions,  
 637 a set of simulations named “waveplus” were defined, where all parameters  
 638 remained unaltered, except the waves (Table 4). According to Costa et al. (2001),  
 639 the joint probability of  $H_s = 1 - 3$  m and  $T_p = 7 - 11$  s is 8.5%, whilst the joint  
 640 probability of  $H_s = 3 - 5$  m and  $T_p = 11 - 15$  s is only 0.1%. Nine conditions were  
 641 modelled and replicated six times, progressing from the baseline model to low-  
 642 probability conditions with  $H_s$  of 4 m and  $T_p$  of 15 s (waveplus 9). Since this test  
 643 aimed to observe increased overwash magnitudes, only peak high-tide water levels  
 644 ( $z = 0.88$  m MSL) were considered. During these simulations, the barrier remained  
 645 in the overwash regime and not in the inundation regime (as defined by Sallenger,  
 646 2000) and the barrier crest was not permanently submerged.

647

648 **Table 4 – Significant wave heights and peak periods for the “waveplus” simulations.**

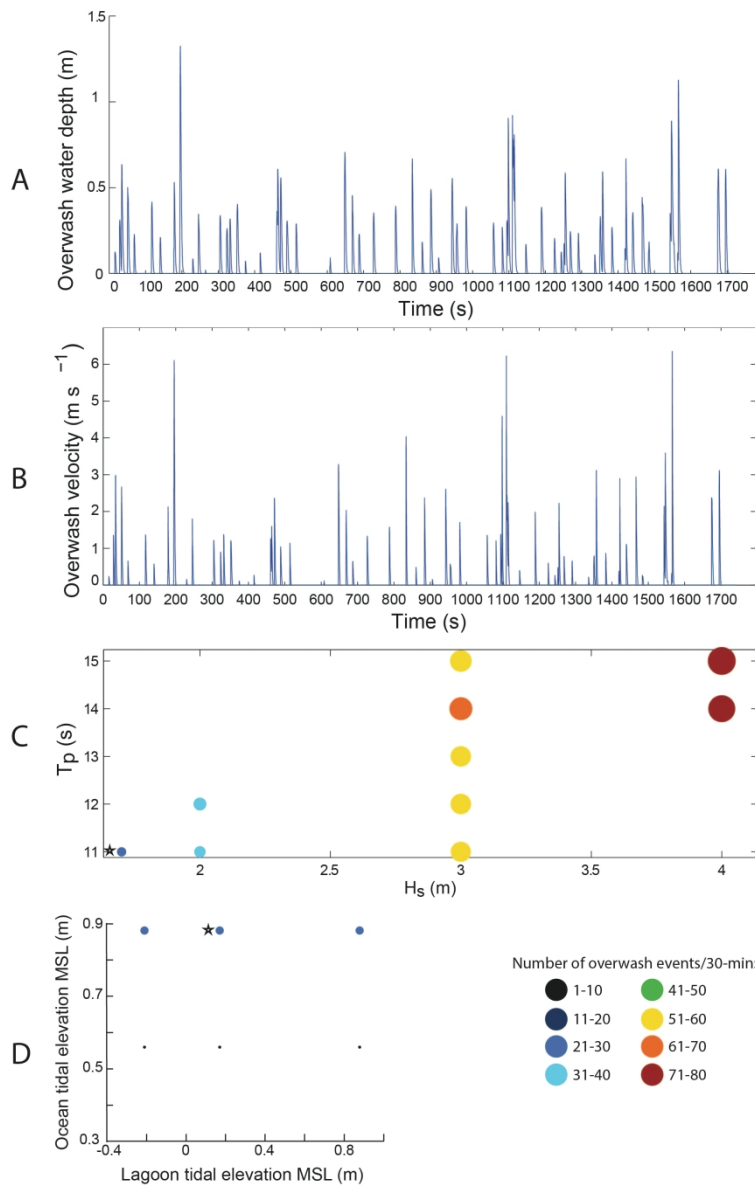
|            | Hs   | Tp   | Probability (%)* |
|------------|------|------|------------------|
| Baseline   | 1.68 | 11.1 |                  |
| waveplus 1 | 2    | 11   | 8.5              |
| waveplus 2 | 3    | 11   |                  |
| waveplus 3 | 2    | 12   |                  |
| waveplus 4 | 3    | 12   | 5.3              |
| waveplus 5 | 3    | 13   |                  |
| waveplus 6 | 3    | 14   | 0.1              |

|            |   |    |
|------------|---|----|
| waveplus 7 | 3 | 15 |
| waveplus 8 | 4 | 14 |
| waveplus 9 | 4 | 15 |

649 \*According to data from Costa et al. (2001).

650

651 For the most extreme conditions simulated, overwash maximum depth can reach up  
652 to 1 m (Figure 13A), which is only comparable to the field dataset of Fisher and  
653 Stauble (1977) that reported overwash induced by Hurricane Belle on Assateague  
654 Island (USA). Maximum overwash velocities reach  $9 \text{ ms}^{-1}$ , which are very high  
655 compared to typical measurements in the field (around  $2 \text{ ms}^{-1}$ , Matias and  
656 Masselink, 2017) and maximum leading edge velocities measured in the field ( $6 \text{ ms}^{-1}$   
657 this study and fieldwork of Almeida et al., 2017), and comparable to the maximum  
658 velocities measured in the laboratory ( $10 \text{ ms}^{-1}$ ; Matias et al., 2014). Average  
659 overwash depth and velocity under extreme wave conditions does not increase as  
660 much as maximum overwash depth and velocity because the number of smaller  
661 overwash events also increases. The percentage of time when seawater is  
662 overtopping the crest is high, particularly for the bigger waves (about 58% of time,  
663 Figure 13). The results show that for each wave height case that was modelled, there  
664 was only a small increase in the number of overwash events with longer peak wave  
665 periods (Figure 13).



666

667 **Figure 13 – Time-series of overwash depth (A) and overwash velocity (B) for one of the replicates**  
 668 **of series waveplus, run 9 ( $H_s = 4$  m;  $T_p = 15$  s). C. Comparison between different waveplus models**  
 669 **with varying  $H_s$  and  $T_p$ . D. Comparison between different lagoon water level tests. The circle size is**  
 670 **proportional to the number of overwash events. The stars identify the baseline model.**

671

672 To test the importance of lagoon levels in overwash occurrence, the model was run  
 673 with the maximum ocean and lagoon water level difference for the fieldwork  
 674 campaign. The baseline model hydraulic gradient was always negative (between -  
 675 0.0054 and -0.0132, towards the lagoon), because the lagoon levels were  
 676 consistently lower. To test other situations, high, mean and low lagoon water levels

677 cases were implemented ( $z = 0.88, 0.17$  and  $-0.21$  m MSL), with two ocean water  
678 levels ( $z = 0.88$  and  $0.56$  m MSL). These changes generated model simulations with  
679 the highest hydraulic gradient ( $0.006$ ) for the high lagoon model and a minimum  
680 hydraulic gradient ( $-0.01$ ) for the lagoon low-tide model, during oceanic high-tide.  
681 Even if the lagoon water level could be lowered, the hydraulic gradients would not  
682 change significantly because of the backbarrier morphology (Figure 2A). As the  
683 water level reaches the backbarrier low-tide flat, a small change in elevation implies  
684 a great increase in horizontal distance, thus lowering the gradient. The results of the  
685 high lagoon, low lagoon and the baseline models present small average variations  
686 (Figure 13C). The average variation in overwash number between the lagoon  
687 models was only 1 event, for both oceanic tidal elevations, which is not statistically  
688 significant. Note however that greater differences in morphodynamic response of  
689 the back barrier may occur, particularly during larger overwash events, as a result  
690 of changing hydraulic gradients between the ocean and lagoon (e.g., Suter et al.,  
691 1982; Donnely et al., 2006; McCall et al., 2010).

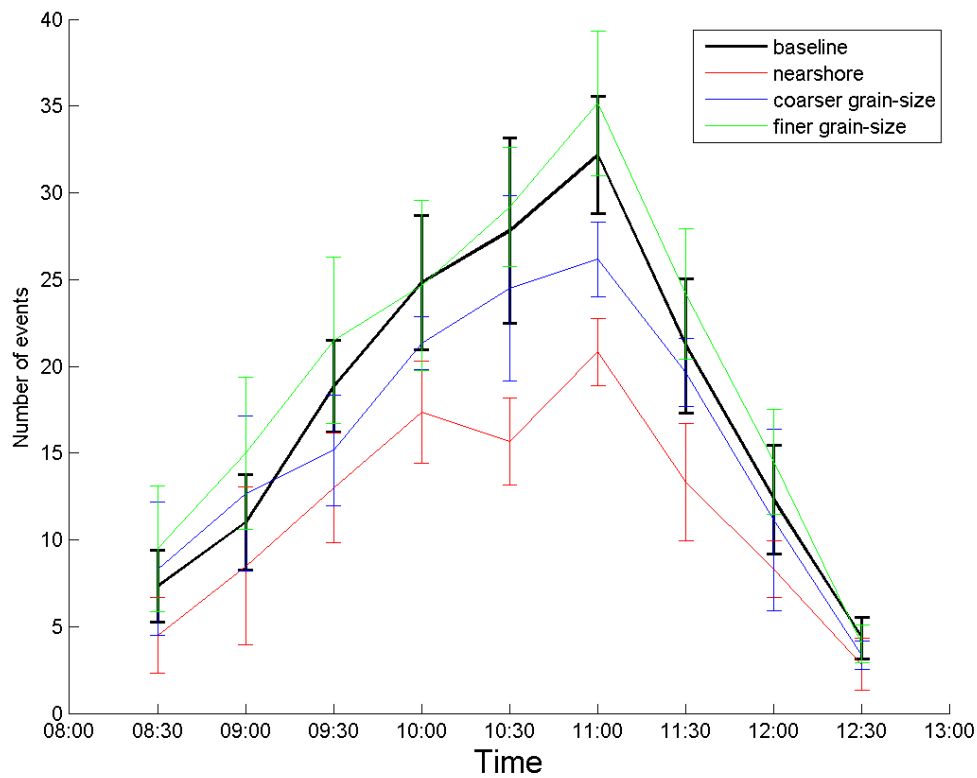
692

## 693 **6.2. BARRIER PARAMETERS**

694 The nearshore morphology is known to change significantly in the study area (e.g.  
695 Vila-Concejo et al., 2006), as a consequence of the migration of swash bars from the  
696 updrift Ancão Inlet. Several nearshore morphological configurations of the study  
697 area were available (data from Matias et al., 2014, also mentioned in section 5.3,  
698 Figure 10) and the one that deviates most from the configuration during the  
699 December 2013 overwash episode was selected for modelling overwash. The survey  
700 in June 2012 showed a significantly higher nearshore bar crest in comparison to the

701 configuration used for the baseline model (Figure 10). The new bathymetric grid  
 702 was built with the same resolution and dimensions of the baseline model, and the  
 703 same oceanographic forcing was superimposed, which implied new SWAN runs  
 704 over the new bathymetric grid.

705 Significant differences are observed between the baseline model and the model with  
 706 a modified nearshore bathymetry (termed “nearshore model”; Figure 14). There is  
 707 a noticeable reduction in the number of overwash events with the nearshore model  
 708 compared to the baseline model, from 160 to 105 events, particularly evident during  
 709 high-tide when the reduction reaches more than 40%.

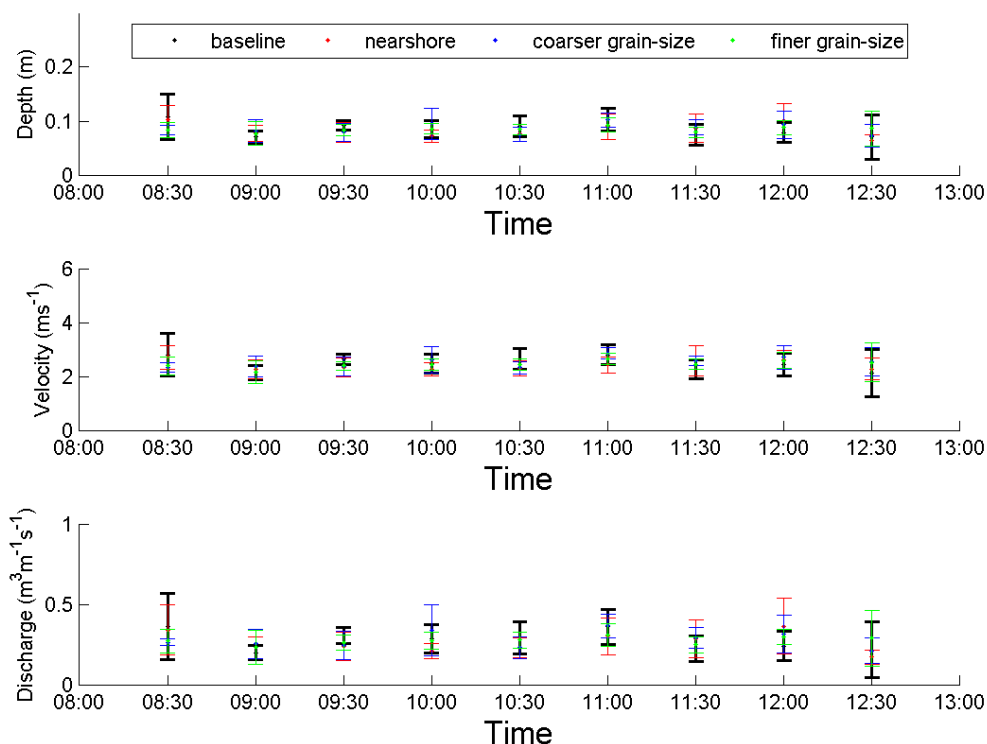


710

711 **Figure 14 – Average and standard deviation of overwash number of events for each time-step of the**  
 712 **baseline model, nearshore model, coarser and finer grain-size models.**

713

714 The average overwash depth, velocity and discharge are also different under the two  
 715 configurations, but the reduction is relatively small (-2 mm average depth, -0.06 ms<sup>-1</sup>  
 716 <sup>1</sup> overwash velocity and -0.01 m<sup>3</sup>m<sup>-1</sup>s<sup>-1</sup>; Figure 15). Overall, overwash water  
 717 discharge during the entire episode for the baseline model was 45 m<sup>3</sup>m<sup>-1</sup> (summing  
 718 the discharges of 160 events) while for the nearshore model this was 27 m<sup>3</sup>m<sup>-1</sup>  
 719 (total of the 105 events) which corresponds to a 40% reduction, mostly due to  
 720 decrease in number of overwash events. The runup statistics (not shown here)  
 721 evidence a reduction in runup on the nearshore model ( $R_{sig}$  decreased 0.22 m in  
 722 relation to baseline model). Average  $R_{sig}$  of the nearshore model is, however, closer  
 723 to fieldwork than the baseline model because it is truncated by the barrier crest  
 724 elevation.



725

726 **Figure 15 – Average depth and velocity of overwash events during each time-step of baseline model,**  
 727 **nearshore model, coarser and finer grain-size models. Average number of events for each time-step**  
 728 **of the baseline model and the different grain-size models.**

729

730 Previous studies in Barreta Island (Matias et al., 2009) indicated variability of  
731 barrier grain-size, both on the beach face and in the barrier washovers. This  
732 information was used to obtain a measure of the likely grain-size variability and  
733 hence set the finer and coarser grain-size models. The finer grain-size model was set  
734 with  $D_{50} = 0.47$  mm, which implied a change of  $K$  to  $0.001 \text{ m s}^{-1}$ , whilst the coarser  
735 grain-size model was set with  $D_{50} = 0.89$  mm and  $K=0.0039 \text{ m s}^{-1}$  (Table 5).

736

737 **Table 5 – Grain-size parameters ( $D_{50}$  and  $D_{10}$ ) and hydraulic conductivity ( $K$ ).**

|           | $D_{50}$ (m) | $D_{10}$ (m) | $K$ (m/s) |
|-----------|--------------|--------------|-----------|
| Fieldwork | 0.00061      | 0.00039      | 0.0015    |
| Coarser*  | 0.00089      | 0.00063      | 0.0039    |
| Average*  | 0.00065      | 0.00041      | 0.0017    |
| Finer*    | 0.00047      | 0.00032      | 0.0010    |

738 \*According to data from Matias et al. (2009).

739

740 The comparison between the baseline model and the finer and coarser grain-size  
741 models showed that the finer grain-size model was the one producing more  
742 overwash, while the coarse grain-size model led to a decrease in overwash number  
743 (Figure 14), probably due to enhanced infiltration. The change in overwash events  
744 was significant, from 160 in the baseline model to 178 in the finer model and 142 in  
745 the coarser model. Again, the changes were particularly evident in the number of  
746 overwash events comparing to the other hydrodynamic variables (depth and  
747 velocity changes were always smaller than 1 mm and  $0.03 \text{ ms}^{-1}$ , respectively; Figure  
748 15). Overall discharges reduced 8% in the coarser and increased 7% in the finer  
749 grain-size models in relation to the baseline model.  $R_{\text{sig}}$  of coarser grain-size model

750 decreased 0.03 m in relation to baseline, while average  $R_{sig}$  of finer grain-size model  
751 increased in 0.01 m.

752

## 753 **7. DISCUSSION**

754 Overall, morphological changes and hydrodynamic parameters observed during the  
755 12<sup>th</sup> of December 2013 overwash episode in Barreta Island compare well with  
756 recent field and laboratory measurements of overwash dynamics. Small  
757 morphological changes, characterized by sediment erosion across the subaerial  
758 beach, but only partially deposited on the barrier top, suggest offshore sediment  
759 transport to the sub-tidal section of the profile of at least part of the eroded  
760 sediment. Similar morphological evolution was observed in recent high-resolution  
761 2D laser scanner measurements of overwash by Almeida et al. (2017). In terms of  
762 hydrodynamic parameters, the most common overwash flow during the overwash  
763 episode was very shallow (mean depth of 0.067 m) and relatively fast, with peak  
764 velocities in the range 1 – 3  $ms^{-1}$ . Such supercritical flows agree with typical  
765 fieldwork and laboratory measurements that can be found in Matias and Masselink  
766 (2017).

767 Because field measurements are scarce and difficult to obtain, and laboratory  
768 datasets may have scale and applicability limitations, reliable numerical models  
769 simulating overwash are valuable to complement field data (e.g. Matias et al., 2017),  
770 While there were limitations in data collection, given the energetic nature of  
771 overwash conditions, the field measurements obtained in Barreta Island  
772 complement the scarce datasets that are available to test numerical models that  
773 simulate overwash (Matias et al., 2017). This innovative field dataset was

774 complemented with published data from overwash on Barreta Island and used to  
775 setup a baseline model of overwash hydrodynamics using XBeach in non-  
776 hydrostatic mode, expanding the evidence base of the model's ability to reproduce  
777 hydrodynamic processes during overwash at field-scale. The baseline model  
778 replicates have a maximum of 18% variation in overwash number, and 40%, 27%  
779 and 100% maximum variation in average overwash depth, velocity and discharge  
780 for 30-minute simulations, respectively. Such large variability between replicates  
781 (standard deviation on number of overwash events= 10-17) clearly evidence the  
782 need for replication when using wave-resolving models to compute representative  
783 statistical properties. Moreover, it demonstrates how field/buoy measurements  
784 condensed in wave spectra, instead of the actual sequence of surface wave  
785 elevations, can represent slightly different conditions and thus translate into  
786 variability and uncertainty in simulation of coastal processes.

787 The baseline model performance metrics were assessed by comparison with  
788 fieldwork using established error metrics, namely bias, RMSE and SCI (McCall et al.,  
789 2014). The results indicate that the baseline model has variable skills over the  
790 duration of the overwash episode, performing better during the rising tide than  
791 during the falling tide. The baseline model has a positive bias, therefore  
792 overestimates the number of overwash events, and an overall RMSE = 7 and SCI =  
793 0.27. These differences between predictions and observations may be related to  
794 several factors, mainly related to uncertainty in the field observations. Morphologic  
795 changes occurring during overwash in the submerged, non-monitored part of the  
796 beach profile can influence subsequent overwash hydrodynamics, as nearshore  
797 morphology has been shown to influence the frequency and intensity of overwash  
798 (Ritchie and Penland, 1988; Matias et al., 2014. Moreover, the baseline model was

799 set with the most recent bathymetry in the area, measured in February 2013, 10  
800 months before the overwash fieldwork. Additionally, there is a lack of measured  
801 wave data in the nearshore and swash zones, as only offshore wave parameters  
802 were obtained from observations. Nearshore wave transformation was simulated  
803 with the model SWAN, which is a well-established model for nearshore wave  
804 propagation, but no quantitative validation can be performed with field data as  
805 instruments in stations ST1 and ST3 collapsed or failed during the overwash  
806 episode. However, the qualitative analysis of nearshore wave spectra  
807 transformation (Figure 6) suggests that the results for wave modelling are within  
808 the expected range of changes for shallow waves as they propagate across nearshore  
809 bars. Difference in model skill for the rising and falling tide can be explained by the  
810 small but positive changes in barrier crest, which built up during the rising tide (~5  
811 cm, Figure 9), and small changes in the tide and surge along the coast, meaning the  
812 imposed ocean water level is less accurate in the falling tide than the rising tide.

813 While recognizing the natural limitations in fieldwork measurements during such  
814 energetic events, as well as various possible sources of error and uncertainties in  
815 model implementation, it was considered that the baseline model provided a  
816 reasonable agreement with field data, which is substantiated by the performance  
817 metrics and by the six additional verification cases. Encouraging results of XBeach  
818 implementation for overwash investigation were also obtained by McCall et al.  
819 (2010) on a sandy beach, Almeida et al. (2017) on a gravel beach and Masselink et  
820 al. (2014) in laboratory experiments. The fieldwork case, i.e., the baseline model was  
821 set without tuning parameters and relying on default XBeach parameterizations,  
822 implemented solely based in data from previous fieldwork (e.g. bathymetry), local  
823 data published in the literature (e.g., offshore bed grain-size), empirical relations

824 (e.g. between grain-size and hydraulic conductivity) and wave modelling (SWAN  
825 model). This methodology is not, however, free of intrinsic and extrinsic errors,  
826 since there is significant inter- and intra-annual variability of bathymetry,  
827 topography and grain-size (e.g., Vila-Concejo et al., 2002; Matias et al., 2004) and  
828 empirical relations used in morphodynamic and wave modelling are also  
829 approximations to real physical conditions.

830 To evaluate the contribution of the several factors locally influencing overwash  
831 hydrodynamics based on modelling results, several case models were simulated  
832 with different ocean conditions and barrier variables, all within the natural  
833 variability of the area. The probability of joint distribution of wave height and period  
834 published in the literature was used to simulate overwash under more energetic and  
835 infrequent oceanographic conditions (the “waveplus” models). Results suggest that  
836 modelled overwash number is more sensitive to changes in the wave height than  
837 variations in wave period, which may be related to the limited range of wave heights  
838 and periods used for this simulation. For instance, laboratory measurements made  
839 by Matias et al. (2012) showed a significant increase of overwash frequency when  
840 the wave period was manipulated on controlled flume experiments. However, due  
841 to its NW-SE orientation (Figure 1), Barreta Island is not exposed to local sea  
842 conditions, which occur under SE winds and typical wave periods of 4-6 s, and only  
843 to SW swell waves trigger overwash events in this area. Therefore, overwash  
844 occurrence under the combination of high waves with shorter periods is not  
845 registered and hence not included in the current analysis.

846 Results show that fieldwork conditions, more frequent and within acceptable safety  
847 and logistic requirements, were relatively mild compared with the possible  
848 overwash magnitude with higher and longer period waves (Figure 13). According

849 to modelling results, oceanographic conditions with a probability of about 0.1 %,  
850 can induce overwash episodes 3-4 times more intense. The low frequency of these  
851 events and fieldwork safety restrictions under these extreme conditions limits the  
852 acquisition of field measurements for the conditions when modelled overwash  
853 velocities peak over  $8 \text{ ms}^{-1}$ . Even under relatively shallow flows, less than 1 m depth  
854 in the waveplus 9 case, these supercritical flows may discharge more  $7 \text{ m}^3\text{m}^{-1}\text{s}^{-1}$ ,  
855 which are beyond acceptable safety levels for people and instrument deployment on  
856 the coast. This means that future application of the baseline model to predict  
857 overwash occurrence and hydrodynamics will be more sensitive to uncertainties in  
858 the predictions of significant wave height, and less sensitive to uncertainties in  
859 predictions of peak wave period, considering the range of observed values the study  
860 area.

861 The ocean tidal level is a fundamental factor in the occurrence of overwash, and it is  
862 included in all runup equations, overwash empirical relations and numerical model  
863 predictions. However, the role of the lagoon tidal level in overwash hydrodynamics  
864 was not established in this area. The modelled cases “lagoon high” and “lagoon low”  
865 were set to cover positive and negative hydraulic gradients that did not occur during  
866 fieldwork (and are impossible to measure in the study area due to its present  
867 configuration, distance to the inlet, backbarrier tidal flat morphology, etc.), but that  
868 could produce relevant contrasting scenarios that enhance the insights that can be  
869 obtained from model simulations. Assuming that the model reproduces correctly  
870 the groundwater flows, results from this study suggest that the lagoon water  
871 elevation has little effect (less than 1%) on overwash hydrodynamics (Figure 13).  
872 Almeida et al. (2017) implementation of Xbeach model on a gravel barrier also  
873 found that groundwater gradients do not produce a significant difference in

874 modelled overwash discharges. This implies that in a data scarce situation, efforts  
875 to obtain accurate predictions or observations of lagoon tidal level are not as  
876 relevant as other parameters to enhance model performance.

877 The contribution of barrier morphological characteristics to overwash  
878 hydrodynamics was also evaluated in this study. Barrier topography, particularly  
879 barrier crest elevation but also beach slope, are critical factors that are included in  
880 all current methods to predict overwash. For example, the role of beach morphology  
881 was found to be crucial in modelling wave overtopping with XBeach by Phillips et al.  
882 (2017), in an area of North Wales, U.K., where exposure to coastal flooding hazards  
883 are significant. In our study, the nearshore bathymetry was also evaluated by setting  
884 the “nearshore model”, which was identical to the baseline model except for the  
885 bathymetry that was changed to the surveyed morphology that differs mostly from  
886 the baseline configuration and is characterized by a more pronounced nearshore  
887 bar. Results indicate an average difference of about 30% of overwash events, with  
888 the nearshore model inhibiting overwash (Figure 14). Based on these results, it was  
889 considered that the nearshore bar, particularly wave transformation and dissipation  
890 that occurs as waves propagate over the nearshore bar, is an important factor in  
891 overwash hydrodynamics. Nearshore morphological variability in this area is  
892 significant, given the detachment and longshore migration of swash bars from the  
893 updrift Ancão Inlet, and therefore accurate and updated bathymetry is paramount  
894 for model performance and accuracy.

895 Although the main sedimentary source to the study area is relatively constant  
896 (longshore drift and inlet associated dynamics), some sand grain-size variability has  
897 been observed in the area (Table 5; Matias et al., 2009). The impact on model results  
898 arising from realistic grain-size changes was tested by running the “coarser” and

899 “finer” grain-size models. The cases simulated are all within the same grain-size  
900 class, with a minimal distinction between medium and coarse sand. On average the  
901 coarser grain-size model promoted less overwash (-11% overwash events number  
902 and -8% discharge), than the baseline model. An intensification of overwash was  
903 recorded with the finer grain-size model. This means that there may be small to  
904 moderate overwash hydrodynamic changes in the study area induced solely by a  
905 relatively limited natural grain-size variability. Previous work in a longshore  
906 variable setting showed that 2D modelling can significantly increase model accuracy  
907 in case of complex bathymetric configurations (e.g. Lerma et al., 2017).

908

909

## 910 **8. CONCLUSION**

911 Data from an overwash episode in Barreta Island (Portugal) are presented in this  
912 study. The overwash episode occurred during mid-tide to high-tide (maximum  
913 oceanic tidal elevation of 0.9 m above MSL), with bimodal waves that resulted from  
914 the combination of swell waves with variable periods and heights. During this  
915 moderate energy event, overwash was not prevalent along most of the Ria Formosa  
916 barrier islands as wave runup was consistently lower than dune crest elevation.  
917 However, in the fieldwork study site (a low-lying barrier stretch) experienced more  
918 than 100 overwash events. Fieldwork observations, modelled nearshore wave  
919 spectra and published data on overwash dynamics in Barreta Island were used to  
920 setup XBeach in non-hydrostatic mode and develop a baseline model of overwash  
921 hydrodynamics. The baseline model was verified against field data, demonstrating  
922 a good agreement according to standard metrics for model performance (bias, RMSE

923 and SCI), with maximum errors of 20% to 25% error for different overwash  
924 variables. Overall, there was an 83% agreement between observed and predicted  
925 overwash episodes.

926 Using recent observations of hydrodynamic forcing and morphological changes for  
927 the area, a set of realistic scenarios was modelled to test the contribution of different  
928 variables for overwash hydrodynamics. Results indicate that the wave height is the  
929 factor that influenced model results the most (up to 400%), followed by the  
930 nearshore bathymetry (up to 30%) and to a lesser extend grain-size (up to 11%).  
931 The relatively small impact of some parameters considered crucial on runup and  
932 overwash, such as wave period, is due to the natural small range of realistic wave  
933 periods that are observed during storms in the study area. This implies that  
934 confidence in model predictions is mainly dependent on the quality of wave height  
935 and water level boundary conditions imposed on the model, as well as up-to-date  
936 barrier parameters, primarily the nearshore bathymetry and barrier configuration  
937 and also the grain-size.

938

## 939 **ACKNOWLEDGEMENTS**

940 This study was supported by RUSH project, PTDC/CTE-GIX/116814/2010 and  
941 EVREST project, PTDC/MAR-EST/1031/2014, financed by FCT, Portugal. A. Matias  
942 and A. Pacheco were supported by Investigator Programme, IF/00354/2012 and  
943 IF/00286/2014, respectively, financed by FCT, Portugal. A.R. Carrasco was  
944 supported by SFRH/BPD/88485/2012. Carlos Loureiro is funded by the EU H2020  
945 MSCA research project NEARControl (Grant Agreement No 661342). T. Plomaritis  
946 was funded by the EU FP7 research project RISC-KIT (ref. RISC-KIT-GA-2013-

947 603458). R. McCall was funded by the EU FP7 RISC-KIT project and Deltares  
948 Strategic Research in the “Hydro-and morphodynamics during extreme events”  
949 program (1230002). Umberto Andriolo was supported by the EARTHSYSTEM  
950 Doctorate Programme led by Institute Dom Luiz Associate Laboratory at the  
951 University of Lisbon (SFRH/BD/52558/2014).

952

953

#### 954 **REFERENCES**

955 Almeida, L.P., Masselink, G., McCall, R., Russell, P., 2017. Storm overwash of a gravel  
956 barrier: field measurements and XBeach-G modelling. *Coastal Engineering*, 120,  
957 22-35.

958 Andriolo U, Almeida LP, Almar R. 2018. Coupling terrestrial LiDAR and video  
959 imagery to perform 3D intertidal beach topography, *Coastal Engineering*, 140,  
960 232-239.

961 Atkinson, A. L., Power, H. E., Moura, T., Hammond, T., Callaghan, D. P., Baldock, T. E.,  
962 2017. Assessment of runup predictions by empirical models on non-truncated  
963 beaches on the south-east Australian coast. *Coastal Engineering*, 119, 15-31.

964 Baldock, T.E., Hughes, M.G., Day, K., Louys, J., 2005. Swash overtopping and  
965 sediment overwash on a truncated beach. *Coastal Engineering*, 52, 633-645.

966 Baumann, J., Chaumillon, E., Bertin, X., Schneider, J.-L., Guillot, B., Schmutz, M.,  
967 2017. Importance of infragravity waves for the generation of washover  
968 deposits. *Marine Geology*, 391, 20-35.

969 Blenkinsopp, C., Matias, A., Howe, D., Castelle, B., Marieu, V., Turner, I., 2016. Wave  
970 runup and overwash on a prototype-scale sand barrier. *Coastal Engineering*,  
971 113, 88-103.

972 Blott, S.J. and Pye, K., 2001. GRADISTAT: a grain size distribution and statistics  
973 package for the analysis of unconsolidated sediments. *Earth Surface Processes*  
974 *and Landforms*, 26, 1237-1248.

975 Booij, N., Ris, R.C., Holthuijsen, L.H., 1999. A third-generation wave model for  
976 coastal regions: 1. Model description and validation. *Journal of Geophysical*  
977 *Research*, C4, 104, 7649-7666.

978 Bouquet, J.Y., 2007. Camera Calibration Toolbox for Matlab. Available in:  
979 <http://www.vision.caltech.edu/bouquetj/calibdoc/>.

980 Bray, T.F. and Carter, C. H. 1992. Physical processes and sedimentary record of a  
981 modern, transgressive, lacustrine barrier island. *Marine Geology*, 105, 155-168.

982 Cleary, W. J., McLeod, M. A., Rauscher, M. A., Johnston, M. K., Riggs, S. R., 2001.  
983 Beach nourishment on hurricane impacted barriers in Southeastern North  
984 Carolina, USA: Targeting shoreface and tidal inlets sand resources. *Journal of*  
985 *Coastal Research* SI 34, 232-255.

986 Costa, M., Silva, R., Vitorino, J., 2001. Contribuição para o estudo do clima de  
987 agitação marítima na costa portuguesa. *Proceedings of 2as Jornadas*  
988 *Portuguesas de Engenharia Costeira e Portuária, International Navigation*  
989 *Association PIANC, Sines, Portugal (in Portuguese)*.

990 Deltares, 2014. XBEACH-G – Storm impact model for gravel beaches: user manual,  
991 at: <https://oss.deltares.nl/web/xbeach/xbeach-og>

992 De Vet, P.L.M., R.T. McCall, J.P. Den Bieman, M.J.F. Stive and M. Van Ormondt  
993 (2015). Modelling dune erosion, overwash and breaching at Fire Island (NY)  
994 during Hurricane Sandy. Proceedings of Coastal Sediments 2015, San Diego,  
995 USA, 11-15 May 2015.

996 Dolan, R. and Godfrey, P., 1973. Effects of Hurricane Ginger on the barrier islands  
997 of North Carolina. Geological Society of America Bulletin, 84, 1329-1334.

998 Donnelly, C., Kraus, N., Larson, M., 2006. State of knowledge on measurement and  
999 modeling of coastal overwash. Journal of Coastal Research, 22(4), 965–991.

1000 Figlus, J., Kobayashi, N., Gralher, C., Iranzo, V., 2011. Wave overtopping and  
1001 overwash of dunes. Journal of Waterway, Port, Coastal, and Ocean Engineering,  
1002 137, 26-33.

1003 Fisher, J.S. and Stauble, D.K., 1977. Impact of Hurricane Belle on Assateague Island  
1004 washover. Geology, 5 (12), 765-768.

1005 FitzGerald, D.M., van Heteren, S., Montello, T.M., 1994. Shoreline processes and  
1006 damage resulting from the Halloween Eve Storm of 1991 along the North and  
1007 South shores of Massachusetts, USA. Journal of Coastal Research, 10, 113-132.

1008 Hughes, M.G., Moseley, A.S., Baldock, T.E., 2010. Probability distributions for wave  
1009 runup on beaches, Coastal Engineering, 57, 575–584.

1010 Gama, C., Dias, J.A., Ferreira, Ó., Taborda, R., 1994. Analysis of storm surge in  
1011 Portugal, between June 1986 and May 1988. Proceedings of the Second  
1012 International Symposium on Coastal Zone Research-Management and Planning,  
1013 EUROCOAST, Lisbon, Portugal, I, 381-387.

- 1014 Leatherman, S.P., 1976. Quantification of overwash processes. Ph.D. Thesis,  
1015 University of Virginia, USA.
- 1016 Lerma, A.N., Pedreros, R., Robinet, A., Sénechal, N., 2017. Simulating wave setup  
1017 and runup during storm conditions on a complex barred beach. *Coastal*  
1018 *Engineering*, 123, 29-41.
- 1019 Lindemer, C.A., Plant, N.G., Puleo, J.A., Thompson, D.M., Wamsley, T.V., 2010.  
1020 Numerical simulation of a low-lying barrier island's morphological response to  
1021 Hurricane Katrina. *Coastal Engineering*, 57, 985-995.
- 1022 Martins, K., Blenkinsopp, C.E., Almar, R., Zang, J., 2017. The influence of swash-  
1023 based reflection on surf zone hydrodynamics: a wave-by-wave approach.  
1024 *Coastal Engineering* 122, 27-43.
- 1025 Masselink, G., McCall, R., Poate, T., van Geer, P., 2014. Modelling storm response on  
1026 gravel beaches using XBeach-G. *Maritime Engineering*, 167, 173-191.
- 1027 Matias, A. and Masselink, G., 2017. Overwash processes: lessons from fieldwork  
1028 and laboratory experiments. In: *Coastal Storms: Processes and Impacts*. (Ed.)  
1029 Paolo Ciavola and Giovanni Coco, John Wiley & Sons Ltd., pp. 175-194.
- 1030 Matias, A., Vila-Concejo, A., Ferreira, Ó., Morris, B., Dias, J.A., 2009. Sediment  
1031 dynamics of barriers with frequent overwash. *Journal of Coastal Research*, 25  
1032 (3), 768-780.
- 1033 Matias, A., Williams, J.J., Masselink, G., Ferreira, Ó. 2012. Overwash threshold for  
1034 gravel barriers. *Coastal Engineering*, 63, 48-61.

1035 Matias, A., Carrasco, A.R., Loureiro, C., Almeida, S., Ferreira, Ó., 2014. Nearshore and  
1036 foreshore influence on overwash of a barrier Island. *Journal of Coastal Research*,  
1037 SI 70, 675-680.

1038 Matias, A., Masselink, G., Castelle, B., Blenkinsopp, C.E., Kroon, A. 2016.  
1039 Measurements of morphodynamic and hydrodynamic overwash processes in a  
1040 large-scale wave flume. *Coastal Engineering*, 113, 33-46.

1041 McCall, R.T., de Vries, J.S.M., Plant, N.G., van Dongeren, A.R., Roelvink, J.A.,  
1042 Thompson, D.M., Reniers, A.J., 2010. Two-dimensional time dependent  
1043 hurricane overwash and erosion modelling at Santa Rosa Island. *Coastal*  
1044 *Engineering*, 57, 668-683.

1045 McCall, R., Masselink, G., Roelvink, D., Russel, P., Davidson, M., Poate, T., 2012.  
1046 Modelling overwash and infiltration on gravel barriers. *Proceedings of the 33<sup>rd</sup>*  
1047 *Conference on Coastal Engineering*, Santander, Spain.

1048 McCall, R.T., Masselink, G., Poate, T.G., Roelvink, J.A., Almeida, L.P., Davidson, M.,  
1049 Russell, P.E., 2014. Modelling storm hydrodynamics on gravel beaches with  
1050 XBeach-G. *Coastal Engineering*, 91, 231-250.

1051 McDonald, J.H. 2014. *Handbook of Biological Statistics (3rd ed.)*. Sparky House  
1052 Publishing, Baltimore, Maryland.

1053 Muller, H.; van Rooijen, A.; Idier, D.; Pedreros, R., Rohmer, J., 2017. Assessing storm  
1054 impact on a French coastal dune system using morphodynamic modeling.  
1055 *Journal of Coastal Research*, 33(2), 254–272.

1056 Pacheco, A., Ferreira, Ó., Carballo, R., Iglesias, G., 2014. Evaluation of the production  
1057 of tidal stream energy in an inlet channel by coupling field data and numerical  
1058 modelling. *Energy*, 71, 104-117.

1059 Pawlowicz, R., Beardsley, B., Lentz, S., 2002. Classical tidal harmonic analysis  
1060 including error estimates in MATLAB using T\_TIDE. Computers & Geosciences,  
1061 28, 929-937.

1062 Phillips, B.T., Brown, J.M., Bidlot, J.R., Plater, A.J., 2017. Role of beach morphology in  
1063 wave overtopping hazard assessment. Journal of Marine Science and  
1064 Engineering, 5, 1.

1065 Popesso C., Pacheco A., Fontolan, G., Ferreira Ó., 2016. Evolution of a relocated inlet  
1066 migrating naturally along an open coast. Journal of Coastal Research, SI (75),  
1067 233-237.

1068 Pessanha, L.E. and Pires, H.O., 1981. Elementos sobre o clima de agitação marítima  
1069 na costa sul do Algarve. Report of Instituto Nacional de Meteorologia e Geofísica.  
1070 66 p. (in Portuguese).

1071 Ris, R.C., Holthuijsen, L.H., Booij, N., 1999. A third-generation wave model for  
1072 coastal regions: 2. Verification. Journal of Geophysical Research, 104, C4, 7667-  
1073 7681.

1074 Ritchie, W. and Penland, S., 1988. Rapid dune changes associated with overwash  
1075 processes on the deltaic coast of South Louisiana. Marine Geology, 81, 97-122.

1076 Roelvink, D., Reniers, A., van Dongeren, A., de Vries, J., McCall, R., Lescinski, J., 2009.  
1077 Modeling storm impacts on beaches, dunes and barrier islands. Coastal  
1078 Engineering, 56, 1133-1152.

1079 Roelvink, D., McCall, R., Mehvar, S., Nederhoff, K., Dastgheib, A., 2017. Improving  
1080 predictions of swash dynamics in XBeach: The role of groupiness and incident-  
1081 band runup. Coastal Engineering, 134, 103-123.

1082 Rosa, F., Rufino, M., Ferreira, Ó., Matias, A., Brito, A.C., Gaspar, M., 2013. The  
1083 influence of coastal processes on inner shelf sediment distribution: The Eastern  
1084 Algarve Shelf (Southern Portugal). *Geologica Acta*, 11, 59-73.

1085 Sallenger, A.H., 2000. Storm impact scale for barrier islands. *Journal of Coastal*  
1086 *Research*, 16 (3), 890-895.

1087 Salmon, J. and Holthuijsen, L., 2015. Modeling depth-induced wave breaking over  
1088 complex coastal bathymetries. *Coastal Engineering*, 105, 21-35.

1089 Smit, P., Stelling, G., Roelvink, J., Van Thiel de Vries, J., McCall, R., Van Dongeren, A.,  
1090 Zwinkels, C., Jacobs, R., 2010. XBeach: Non-hydrostatic model: Validation,  
1091 verification and model description. Technical report. Delft University of  
1092 Technology and Deltares, 59 pp.

1093 Smith, G.A., Babanin, A.V., Riedel, P., Young, I.R., Oliver, S., Hubbert, G., 2011.  
1094 Introduction of a new friction routine into the SWAN model that evaluates  
1095 roughness due to bedform and sediment size changes. *Coastal Engineering*, 58,  
1096 317-326.

1097 Stockdon, H.F., Holman, R.A., Howd, P.A., Sallenger, A.H., 2006. Empirical  
1098 parameterization of setup, swash, and runup. *Coastal Engineering*, 53, 573-588.

1099 Stockdon, H.F., Doran, K.S., Sallenger, A.H., 2009. Extraction of lidar-based dune-  
1100 crest elevations for use in examining the vulnerability of beaches to inundation  
1101 during hurricanes. *Journal of Coastal Research*, SI 53, 59-65.

1102 Stone, G., Liu, B., Pepper, D. A., Wang, P., 2004. The importance of extratropical and  
1103 tropical cyclones on the short-term evolution of barrier islands along the  
1104 northern Gulf of Mexico, USA. *Marine Geology*, 210, 63-78.

- 1105 Suter, J. R., Nummedal, D., A., Maynard, K., Kemp, P., 1982. A process-response  
1106 model for hurricane washovers. Proceedings of 18th Coastal Engineering  
1107 Conference, Capetown, South Africa, pp. 1459–1789.
- 1108 van Dongeren, A., Roelvink, D., McCall, R., Nederhoff, K., van Rooijen, A., 2017.  
1109 Modelling the morphological impacts of coastal storms. In: Coastal Storms:  
1110 Processes and Impacts. (Ed.) Paolo Ciavola and Giovanni Coco, John Wiley &  
1111 Sons Ltd., pp. 195-216.
- 1112 Vila-Concejo, A., Matias, A., Ferreira, Ó., Duarte, C., Dias, J.A., 2002. Recent evolution  
1113 of the natural inlets of a barrier island system in Southern Portugal. Journal of  
1114 Coastal Research, SI 36, 741-752.
- 1115 Vila-Concejo, A., Matias, A., Ferreira, Ó., Dias, J.A., 2006. Inlet sediment bypassing to  
1116 a downdrift washover plain. Journal of Coastal Research, SI 39, 401–405.
- 1117 Vousdoukas, M.I., Wziatek, D., Almeida, L. P., 2011. Coastal vulnerability  
1118 assessment based on video wave run-up observations at a mesotidal, steep-  
1119 sloped beach. Ocean Dynamics, 62(1), 123-137.
- 1120